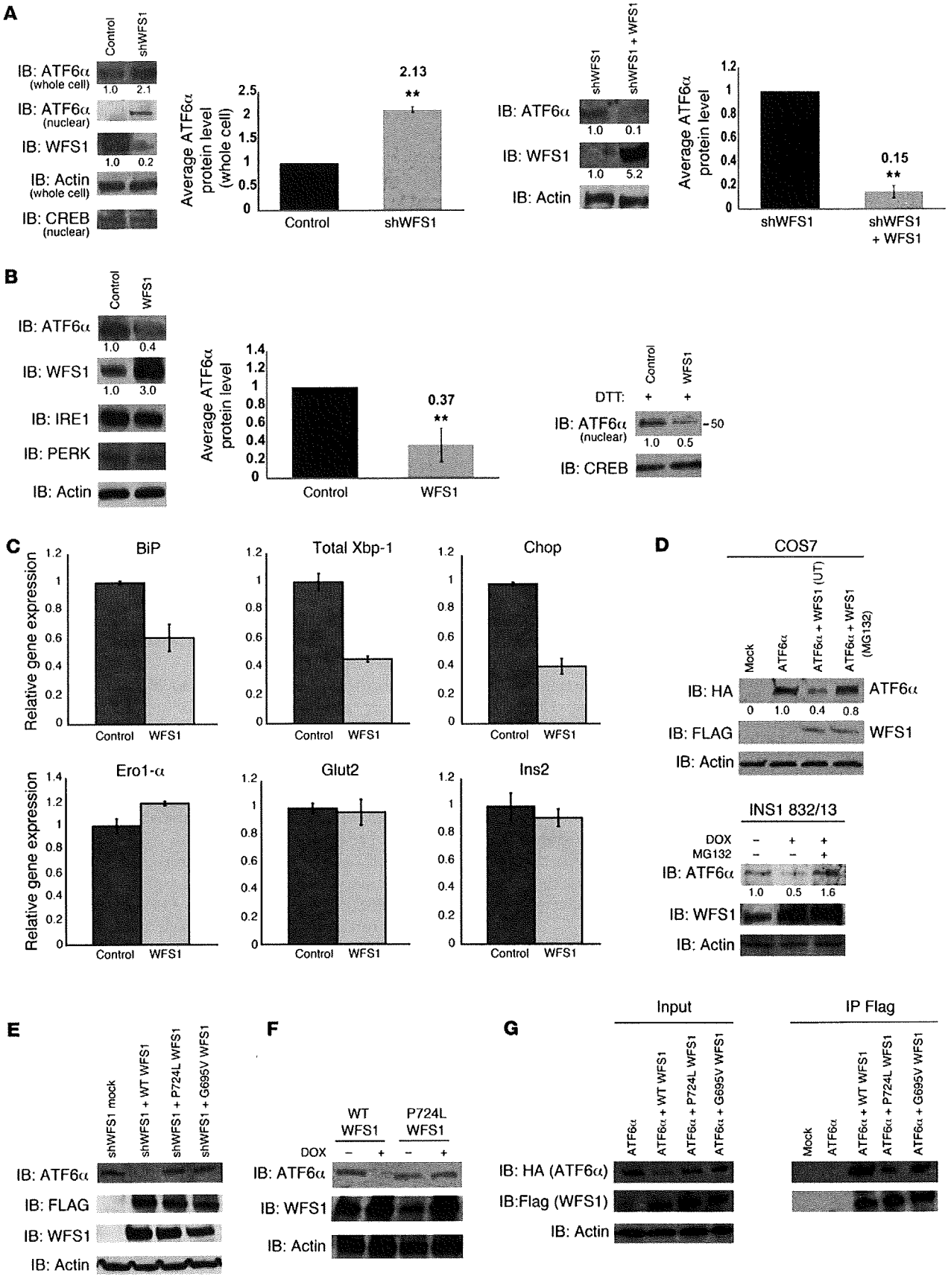
A
Control
shWFS1
IB: ATF6α (whole cell)
1.0 2.1
IB: ATF6α (nuclear)
IB: WFS1
1.0 0.2
IB: Actin (whole cell)
IB: CREB (nuclear)
Average ATF6α protein level (whole cell)
2.13
**
Control
shWFS1
shWFS1
shWFS1 + WFS1
IB: ATF6α
1.0 0.1
IB: WFS1
1.0 5.2
IB: Actin
Average ATF6α protein level
0.15
**
shWFS1
shWFS1 + WFS1
B
Control
WFS1
IB: ATF6α
1.0 0.4
IB: WFS1
1.0 3.0
IB: IRE1
IB: PERK
IB: Actin
Average ATF6α protein level
0.37
**
Control
WFS1
DTT:
IB: ATF6α (nuclear)
1.0 0.5
IB: CREB
C
BiP
Total Xbp-1
Chop
Relative gene expression
Control WFS1
Ero1-α
Glut2
Ins2
D
COS7
Mock
ATF6α
ATF6α + WFS1 (UT)
ATF6α + WFS1 (MG132)
IB: HA
ATF6α
0 1.0 0.4 0.8
IB: FLAG
WFS1
IB: Actin
INS1 832/13
DOX
MG132
IB: ATF6α
1.0 0.5 1.6
IB: WFS1
IB: Actin
E
shWFS1 mock
shWFS1 + WT WFS1
shWFS1 + P724L WFS1
shWFS1 + G695V WFS1
IB: ATF6α
IB: FLAG
IB: WFS1
IB: Actin
F
WT WFS1
P724L WFS1
DOX
IB: ATF6α
IB: WFS1
IB: Actin
G
Input
IP Flag
ATF6α
ATF6α + WT WFS1
ATF6α + P724L WFS1
ATF6α + G695V WFS1
Mock
IB: HA (ATF6α)
IB:Flag (WFS1)
IB: Actin

Figure 2
WFS1 regulates ATF6α protein levels. (**A**) IB analysis measured ATF6α and WFS1 levels in MIN6 cells expressing shGFP (control) or shWFS1, as well as in MIN6 cells expressing shWFS1 or expressing shWFS1 and rescued with WFS1 (n = 3). (**B**) IB analysis measuring ATF6α, WFS1, IRE1α, and PERK levels in INS1 832/13 cells (treated with 2 mM DTT for 3 hours) overexpressing GFP (control) or WFS1 (n = 3). (**C**) Quantitative real-time PCR analysis of BiP, total Xbp-1, Chop, Ero1-α, Glut2, and Ins2 mRNA levels in INS1 832/13 cells overexpressing GFP (control) or WFS1 (n = 3). (**D**) IB analysis of ATF6α and WFS1 in COS7 cells transfected with ATF6α-HA or ATF6α-HA and WFS1-FLAG at 2 different ratios, and in INS1 832/13 cells expressing inducible WFS1 and treated with or without MG132. (**E**) IB analysis of ATF6α and WFS1 in MIN6 cells expressing shWFS1 and transfected with WT WFS1-FLAG or mutant P724L WFS1-FLAG and G695V WFS1-FLAG (n = 3). (**F**) IB analysis measuring ATF6α and WFS1 levels in INS1 832/13 cells expressing WT WFS1 or P724L WFS1 (n = 3). (**G**) WFS1 was subjected to IP from COS7 cells expressing ATF6α-HA or ATF6α-HA with WT, P724L, or G695V WFS1-Flag using an anti-Flag antibody. IPs and input proteins were analyzed using anti-HA and anti-Flag antibodies. $^{**}P < 0.01$.

Both WFS1 and ATF6α are transmembrane proteins localized to the ER (3, 10), raising the possibility that the suppression of the ATF6α reporter by WFS1 might be mediated by direct interaction between the WFS1 and ATF6α proteins. To confirm this, the association of WFS1 with ATF6α was examined in the pancreatic β cell line INS-1 832/13. WFS1 associated with ATF6α under nonstress conditions (Figure 1D). To examine whether this interaction was maintained during ER stress conditions, the cells were treated with the ER stress inducer dithiothreitol (DTT), which caused a dissociation of ATF6α from WFS1 in a time-dependent manner, with almost complete dissociation 3 hours after treatment (Figure 1D). This ER stress–dependent interaction was also observed in cells treated with another ER stress inducer, thapsigargin (Supplemental Figure 1; supplemental material available online with this article; doi:10.1172/JCI39678DS1). To confirm that this interaction was recovered after stress, cells were treated for 2 hours with DTT and then chased in normal media. As expected, the interaction of ATF6 and WFS1 began to recover after a 1-hour chase (Figure 1E). This interaction was also seen in the neuronal cell line Neuro2A (Supplemental Figure 2). Together, these data suggest that ATF6 is released from WFS1 under stress in order to activate its target UPR genes.

WFS1 has a function in the degradation of ATF6α through the ubiquitin-proteasome pathway. Suppression of ATF6α transcriptional activity by WFS1 and the formation of an ATF6α-WFS1 complex led to the prediction that WFS1 regulates ATF6α function at the posttranslational level. To test this prediction, we derived a pancreatic β cell line, MIN6 cells, stably expressing a shRNA directed against WFS1. Full-length as well as nuclear ATF6α protein levels increased approximately 2-fold compared with control cells (Figure 2A). To confirm that upregulation of ATF6α protein is directly regulated by WFS1, we reintroduced a lentivirus expressing WFS1 into the cells expressing shRNA directed against WFS1; ATF6 protein expression levels were again reduced when WFS1 was reintroduced (Figure 2A).

ATF6α mRNA was unchanged in the WFS1-knockdown INS-1 832/13 cells, but ATF6α target genes, such as $p58^{IPK}$ and BiP (7, 8), were upregulated as predicted (Supplemental Figure 3). To further confirm that this upregulation is directly regulated by ATF6α, we suppressed ATF6α expression by siRNA in WFS1 knockdown INS-1 832/13 cells and then measured expression levels of its major target, BiP. Upregulation of BiP by WFS1 inhibition was cancelled out by ATF6α inhibition (Supplemental Figure 4).

ATF6α protein levels were also measured in INS-1 832/13 cells overexpressing WFS1. Full-length and nuclear ATF6α protein levels were suppressed in these cells, whereas there was no significant change in protein levels of the other 2 master regulators of the UPR, IRE1 and PERK (Figure 2B). IRE1 and PERK protein expression levels were not decreased even with higher levels of WFS1 expression (Supplemental Figure 5). Suppression of ATF6α protein expression was also seen in a neuronal cell line (Supplemental Figure 6). ATF6 target gene mRNA levels were also suppressed in β cells overexpressing WFS1 (Figure 2C). The relationship of WFS1 and ATF6 protein expression was found to be dose-dependent: increased expression of WFS1 leads to a decrease in ATF6 protein expression (Supplemental Figure 7). We asked whether this relationship was proteasome dependent. Treatment of 2 WFS1-overexpressing cell lines with the proteasome inhibitor MG132 rescued ATF6α protein levels (Figure 2D). We cloned 2 missense mutants, WFS1 P724L and WFS1 G695V, and 1 inactivating mutant, WFS1 ins483fs/ter544, from patient samples (13). Mutant variants of WFS1 did not affect ATF6α protein levels in MIN6 cells expressing shRNA directed against WFS1 (Figure 2E and Supplemental Figure 8). This was also confirmed in INS-1 832/13 cells expressing the missense mutant WFS1 P724L (Figure 2F) and in neuronal cells expressing the missense mutant WFS1 G695V (Supplemental Figure 9). Although ATF6α weakly interacted WFS1 P724L and WFS1 G695V, there was no significant decrease in ATF6α protein levels in these cells (Figure 2G).

To assess the impact of WFS1 on ATF6α protein degradation, cycloheximide experiments were performed. In MIN6 cells expressing shRNA directed against WFS1, there was a block in ATF6α protein degradation, whereas in cells overexpressing WFS1, there was minimal ATF6α protein expression (Figure 3, A and B). WFS1 could not enhance the degradation of 2 other ER proteins susceptible to misfolding, TCRα and mutant alpha-1-antitrypsin NHK3 (refs. 22–24 and Supplemental Figure 10), which indicates that WFS1 specifically degrades ATF6α protein. WFS1 also enhanced the ubiquitination of ATF6α. In cells expressing shRNA directed against WFS1, there was a decrease in ATF6α ubiquitination after blocking proteasome activity (Figure 3C), whereas in cells overexpressing WFS1, there was an enhancement of ATF6α ubiquitination (Figure 3D). In *Wfs1*$^{-/-}$ mouse pancreata, ATF6α protein expression was strikingly high compared with control littermate pancreata (Figure 3E), indicating that WFS1 functions in ATF6α protein expression in vivo. In samples from patients with WFS1 mutations, there was a higher expression of ATF6α protein compared with control samples (Supplemental Figure 11). Together, these results indicate that WFS1 is important for regulating ATF6α protein expression. When WFS1 was not present, there was increased expression of ATF6α protein and hyperactivation of its downstream effectors. This suggests that in response to ER stress, ATF6α escapes from WFS1-dependent degradation, is cleaved in the Golgi to its active form, and then translocates to the nucleus to upregulate its UPR target genes.

These data raised the possibility that WFS1 recruits ATF6α to the proteasome for its degradation. As we predicted, WFS1 formed a complex with the proteasome (Figure 4A). When glyc-

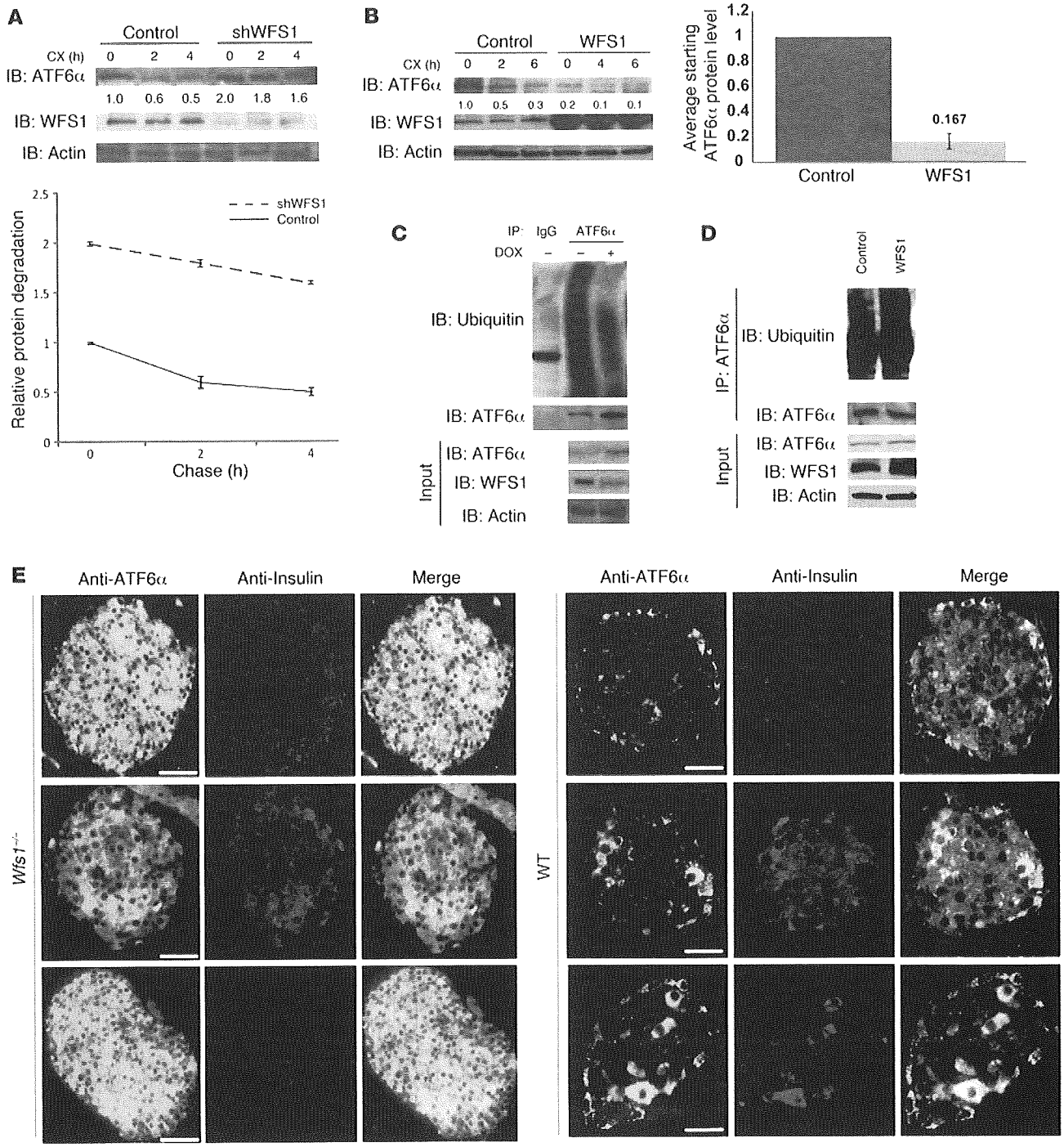

Figure 3

WFS1 enhances ATF6α ubiquitination and degradation. (**A**) IB analysis measuring ATF6α, WFS1, and actin levels in MIN6 cells stably expressing shGFP (control) or shWFS1 treated with 40 μM cycloheximide (CX) for 0, 2, and 4 hours (n = 3). (**B**) IB analysis measuring ATF6α, WFS1, and actin levels in INS1 832/13 cells expressing GFP (control) or WFS1 treated with 40 μM cycloheximide for 0, 2, and 6 hours (n = 3). (**C**) ATF6α was subjected to IP using an anti-ATF6α antibody from an INS1 832/13 cells inducibly expressing shWFS1 (treated for 48 hours with 2 μM doxycycline) and treated with MG132 (20 μM) for 3 hours. IPs were then subjected to IB with anti-ubiquitin and anti-ATF6α antibodies, and input lysates were blotted with anti-ATF6α, anti-WFS1, and anti-actin antibodies (n = 3). (**D**) ATF6α was subjected to IP using an anti-ATF6α antibody, from INS1 832/13 cells overexpressing GFP (control) or WFS1, then treated with MG132 (0.1 μM) overnight. IPs were subjected to IB with anti-ubiquitin and anti-ATF6α antibodies. Input lysates were subjected to IB with anti-ATF6α, anti-WFS1, and anti-actin antibodies (n = 3). (**E**) *Wfs1*$^{-/-}$ and WT littermate mouse pancreata were analyzed by immunohistochemistry using anti-ATF6α and anti-insulin antibodies. Scale bars: 50 μm.

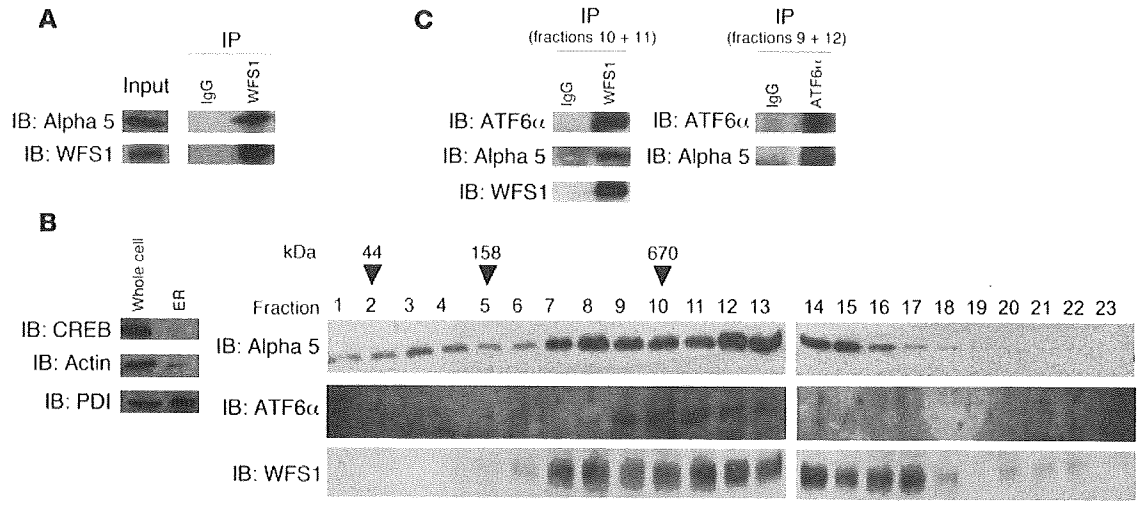

Figure 4

WFS1 forms a complex with the proteasome and ATF6α. (**A**) WFS1 was subjected to IP from INS1 832/13 cells using an anti-WFS1 specific antibody. IPs were subjected to IB with anti–alpha 5 20S proteasome and anti-WFS1 antibodies. (**B**) IB analysis measuring CREB, actin, and PDI levels using whole cell lysates or ER-isolated lysates of INS1 832/13 cells. ER-isolated lysates of INS1 832/13 cells were also subjected to fractionation using a 10%–40% glycerol gradient. Fractions were analyzed by IB using anti–alpha 5 20s proteosome, anti-ATF6α, and anti-WFS1 antibodies. Lanes were run on separate gels and were not contiguous. (**C**) WFS1 was subjected to IP from a mixture of fractions 10 and 11 using an anti-WFS1 antibody, and IP products were subjected to IB analysis using anti-alpha 5 20s proteosome, anti-ATF6α, and anti-WFS1 antibodies. ATF6 was subjected to IP from a mixture of fractions 9 and 12, and IP products were analyzed by IB with anti–alpha 5 20s proteosome and anti-ATF6α (n = 3).

erol-gradient fractionation was performed on ER-isolated lysates, the proteasome ATF6α and WFS1 comigrated in the same high-molecular weight fractions, and a complex between them was formed (Figure 4, B and C).

WFS1 stabilizes HRD1, which functions as an E3 ligase for ATF6α. Because WFS1 is localized to the ER membrane and recruits ATF6α to the proteasome, but is not itself an E3 ligase, we searched for ER-localized E3 ligases with which WFS1 could interact. A top candidate was the ER-resident E3 ligase HRD1, which has a known role in ER stress signaling (25, 26). SEL1/HRD3, which has an important function in hydroxy-3-methylglutaryl-CoA reductase (HMG-R) degradation (27), has been shown to interact with and stabilize HRD1 (28), raising the possibility that WFS1 may also have a similar function and could interact with HRD1. Indeed, WFS1 and HRD1 formed a complex (Figure 5A). We next asked whether WFS1 also plays a role in HRD1 protein expression. Inducible suppression of WFS1 in INS-1 832/13 cells expressing shRNA directed against WFS1 suppressed HRD1 protein expression (Figures 5B). To test the effect of WFS1 on HRD1 protein stability, we performed cycloheximide experiments using MIN6 cells stably expressing shRNA directed against WFS1. HRD1 protein expression was significantly decreased in WFS1 knockdown cells compared with control cells, and it was difficult to measure the stability of HRD1 (Figure 5C).

We further confirmed the effects of WFS1 on HRD1 protein expression in vivo using *Wfs1*$^{-/-}$ mice. As expected from the results using β cell lines, HRD1 expression was undetectable in islets of *Wfs1*$^{-/-}$ mice (Figure 5D). In addition, in samples from patients with Wolfram syndrome, there was less HRD1 protein expression compared with control samples (Supplemental Figure 12A). HRD1 expression did not affect WFS1 protein expression (Supplemental Figure 12B).

We next sought to compare the effects of WT WFS1 and WFS1 mutants on HRD1 protein expression. Ectopic expression of WT WFS1 increased HRD1 protein expression, whereas ectopic expression of missense and inactivating WFS1 mutants did not increase or decrease HRD1 expression (Figure 5E). To determine whether WFS1 mutants interact with HRD1, comparable amounts of WT and missense mutant WFS1 proteins were expressed together with HRD1 in COS7 cells, and the interaction was monitored by co-IP. HRD1 interacted with WT WFS1, but not with WFS1 mutants (Figure 5F). Collectively, these results demonstrated that WFS1 stabilizes and enhances the function of the E3 ligase HRD1 through direct binding.

Based on the ability of WFS1 to regulate ATF6α protein, as well as its function in stabilizing HRD1, it followed that WFS1 may be recruiting ATF6α to HRD1 and that ATF6α is a substrate of HRD1. Indeed, HRD1 interacted with ATF6α (Figure 6A). In glycerol-gradient fractionation experiments of ER-isolated lysates, HRD1, ATF6α, and WFS1 were found to form a complex (Supplemental Figure 13). We next analyzed the interaction between ATF6α and HRD1 under ER stress conditions. ATF6α was released from HRD1 by DTT and thapsigargin treatments (Figure 6B), which indicates that the interaction between these proteins is disrupted by ER stress. To study the relationship between HRD1 and ATF6α protein expression levels, the stability of ATF6α protein was measured in MIN6 cells stably expressing shRNA directed against HRD1 and control cells. HRD1 suppression in cells enhanced ATF6α protein stability (Figure 6C). In contrast, overexpression of HRD1 enhanced ATF6α protein degradation (Figure 6D). HRD1 also enhanced ATF6α ubiquitination, and lack of HRD1 decreased ATF6α ubiquitination (Figure 6, E and F). Collectively, these results indicate that the WFS1-HRD1 complex enhances ATF6α ubiquitination and degradation.

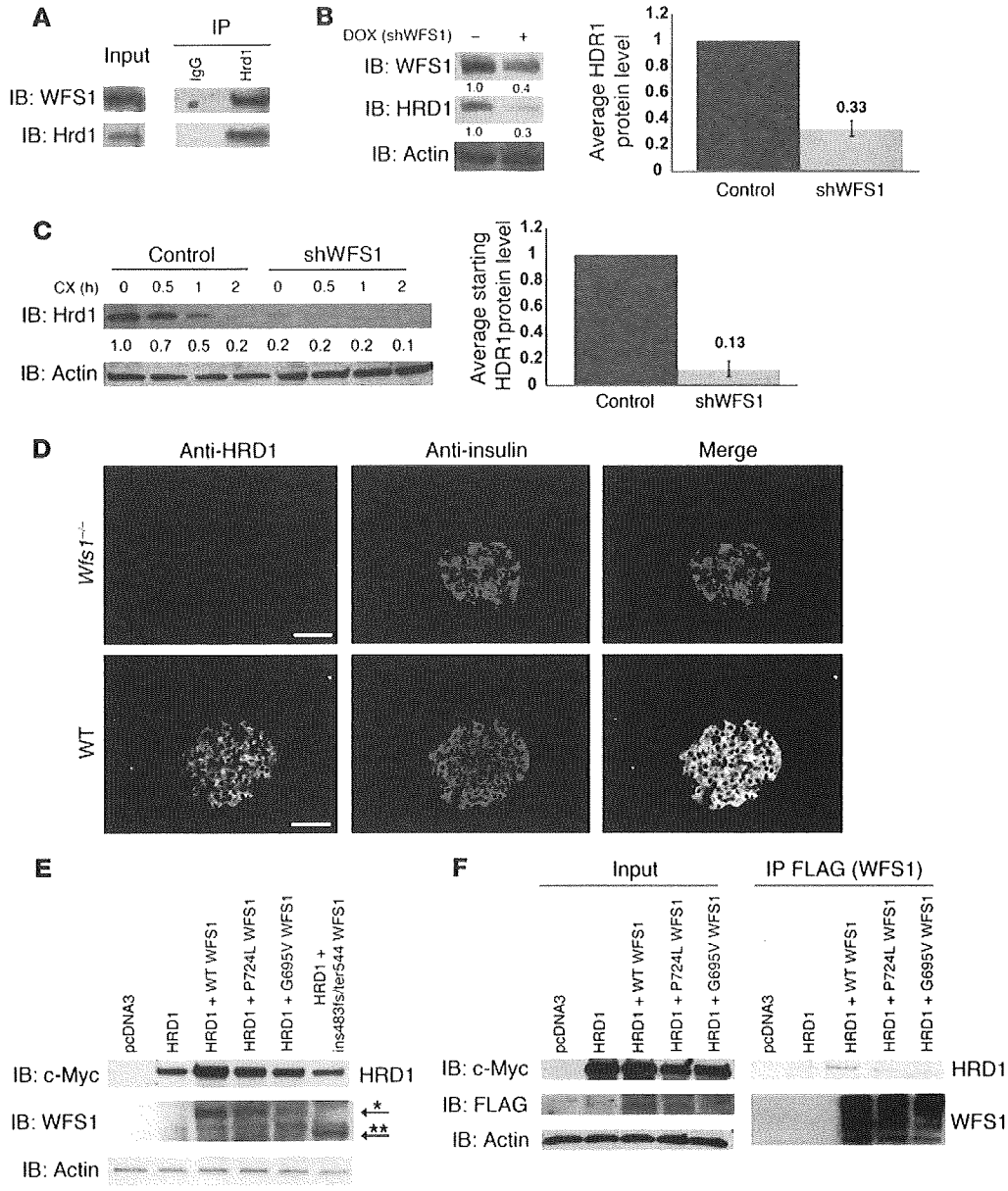

Figure 5

WFS1 interacts with and stabilizes the E3 ligase HRD1. (**A**) Hrd1 was subjected to IP from INS1 832/13 cells, and IPs were subjected to IB analysis using anti-WFS1 and anti-Hrd1 antibodies ($n = 3$). (**B**) Total lysates from INS1 832/13 cells inducibly expressing shWFS1 (treated with 2 μM doxycycline for 48 hours) were analyzed by IB using anti-WFS1, anti-Hrd1, and anti-actin antibodies ($n = 3$). (**C**) IB analysis measuring HRD1 levels in MIN6 cells stably expressing shGFP (control) or shWFS1 treated with 40 μM cycloheximide for 0, 0.5, 1, and 2 hours ($n = 3$). (**D**) *Wfs1*$^{-/-}$ and WT littermate mouse pancreata were analyzed by immunohistochemistry using anti-HRD1 and anti-insulin antibodies ($n = 3$). Scale bars: 100 μm. (**E**) COS7 cells were transfected with pcDNA3, HRD1–c-Myc, HRD1–c-Myc and WT WFS1, or HRD1–c-Myc and WFS1 mutants (P724L, G695V, and ins483fs/ter544) expression plasmids. Expression levels of HRD1–c-Myc, WFS1, and actin were measured by IB using anti–c-Myc, anti-WFS1, and anti-actin antibodies, respectively. WT and mutant WFS1 are denoted by single and double asterisks, respectively. (**F**) COS7 cells were transfected with pcDNA3, HRD1–c-Myc, HRD1–c-Myc and WT WFS1-Flag, HRD1–c-Myc and WFS P724L-Flag, and HRD1–c-Myc and WFS1 G695V-Flag expression plasmids. The lysates were subjected to IP with anti-Flag antibody and IB with anti–c-Myc antibody to study the interaction between HRD1 and WFS1.

Discussion

In this study, we provide evidence that WFS1 plays a crucial role in regulating ATF6α transcriptional activity through HRD1-mediated ubiquitination and proteasome-mediated degradation of ATF6α protein. Based upon the data provided, we propose a pathway for the negative-feedback regulation of the ER stress signaling network by WFS1 (Figure 7). In healthy cells, WFS1 prevents dysregulated ER stress signaling by recruiting ATF6α to HRD1 and the proteasome for ubiquitin-mediated degradation under non–ER stress conditions. When stress is applied to the ER, such as through the chemical ER stress inducer DTT, ATF6α is released from WFS1. It is then released from the ER membrane and translocates to the

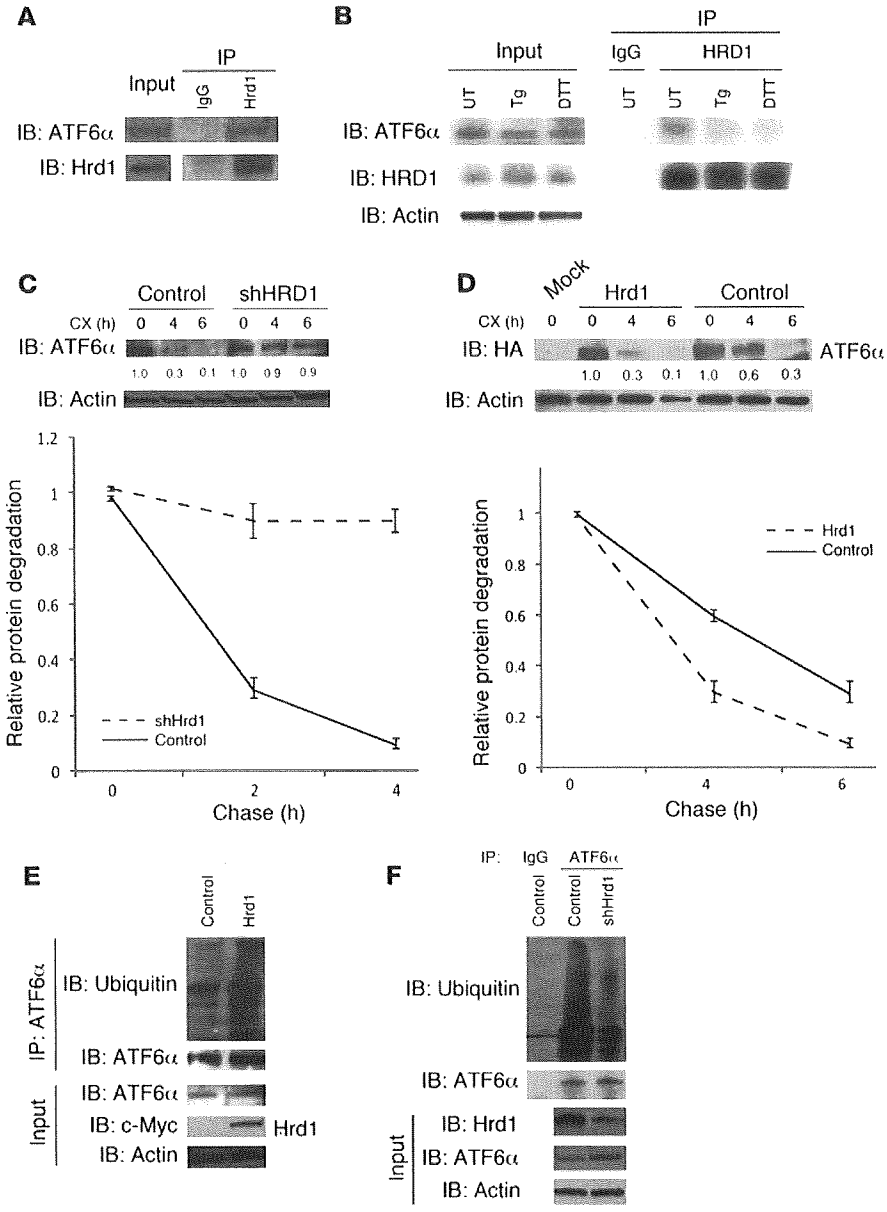

Figure 6

HRD1 is an E3 ligase for ATF6α. (**A**) HRD1 was subjected to IP from INS1 832/13 cells treated for 3 hours with 30 μM MG132. IPs and input proteins were analyzed by IB using anti-ATF6α and anti-HRD1 antibodies. Lanes were run on the same gel but were noncontiguous (white line). (**B**) An anti-HRD1 antibody was used to IP HRD1 protein from INS1 832/13 cells untreated or treated with DTT (1 mM) and thapsigargin (Tg; 1 μM) for 3 hours. IPs were then subjected to IB analysis using anti-ATF6α, anti-HRD1, and anti-actin antibodies (n = 3). (**C**) IB analysis measuring ATF6α levels in MIN6 cells stably expressing shGFP (control) or shRNA shHRD1 treated with 40 μM cycloheximide for 0, 4, and 6 hours (n = 3). (**D**) COS7 cells transfected with ATF6α-HA expression plasmid (control) or ATF6α-HA together with Hrd1-myc expression plasmids (Hrd1) were treated with 40 μM cycloheximide for 0, 4, and 6 hours. Whole cell lysates were subjected to IB with an anti-HA antibody (n = 3). (**E**) ATF6α was subjected to IP using an anti-ATF6α antibody from INS1 832/13 cells either mock transfected (control) or transfected with a Hrd1-Myc expression plasmid and treated with MG132 (20 μM) for 3 hours. IPs were then subjected to IB with anti-ubiquitin and anti-ATF6α antibodies, and input lysates were blotted with anti-ATF6α, anti–c-Myc, and anti-actin antibodies (n = 3). (**F**) ATF6 was subjected to IP using an anti-ATF6α antibody from MIN6 cells stably expressing shGFP (control) or shHRD1 and treated with MG132 (20 μM) for 3 hours. IPs were then subjected to IB with anti-ubiquitin and anti-ATF6α antibodies, and input lysates were blotted with anti-HRD1, anti-ATF6α, and anti-actin antibodies (n = 3).

nucleus, where it upregulates stress signaling targets. At later time points, WFS1 is induced by ER stress, causing eventual degradation of ATF6α when ER homeostasis is established. In patients with Wolfram syndrome or *Wfs1*$^{-/-}$ mice, ATF6α escapes from this proteasome-dependent degradation, leading to dysregulated ATF6α signaling. This ATF6α hyperactivation caused by the lack of WFS1 is probably involved in β cell apoptosis.

It has previously been shown that WFS1-deficient β cells are susceptible to ER stress–mediated apoptosis (11, 18, 29). We confirmed that knockdown of WFS1 made β cells sensitive to ER stress–mediated cell death (Supplemental Figure 14). In addition, we found that ectopic expression of an active form of ATF6α in β cells caused apoptosis (Supplemental Figure 15). Although this fits to our model that hyperactivation of ATF6α has a harmful effect on β cells and leads to apoptosis, it may be contrary to previous studies showing beneficial effects of ATF6α upregulation. For example, it has been shown that activation of the ATF6α pathway by a chemical compound protects neuronal cells from ER stress–mediated apoptosis (30). This effect is mediated by BiP upregulation. The induction of ATF6α has also been shown to protect cardiomyocytes from ischemia/reperfusion-mediated apoptosis (31). This effect is also mediated by BiP and GRP94 upregulation. Conversely, a recent report has shown that ATF6α upregulation attenuates diet-induced obesity and insulin resistance (32). More importantly, it has been shown that WT mice are better protected from ER stress in vivo than are ATF6α knockout mice. ATF6α knockout hepatocytes have been shown to be more sensitive to ER stress–mediated cell death compared with control hepatocytes (7). It is not surprising that previous studies found induction of ATF6α to have beneficial effects on cell function and cell survival, because ATF6α is a major regulator for BiP, a central molecular chaperone in the ER (7, 8). The main conclusion of the present study is that chronic dysregulation

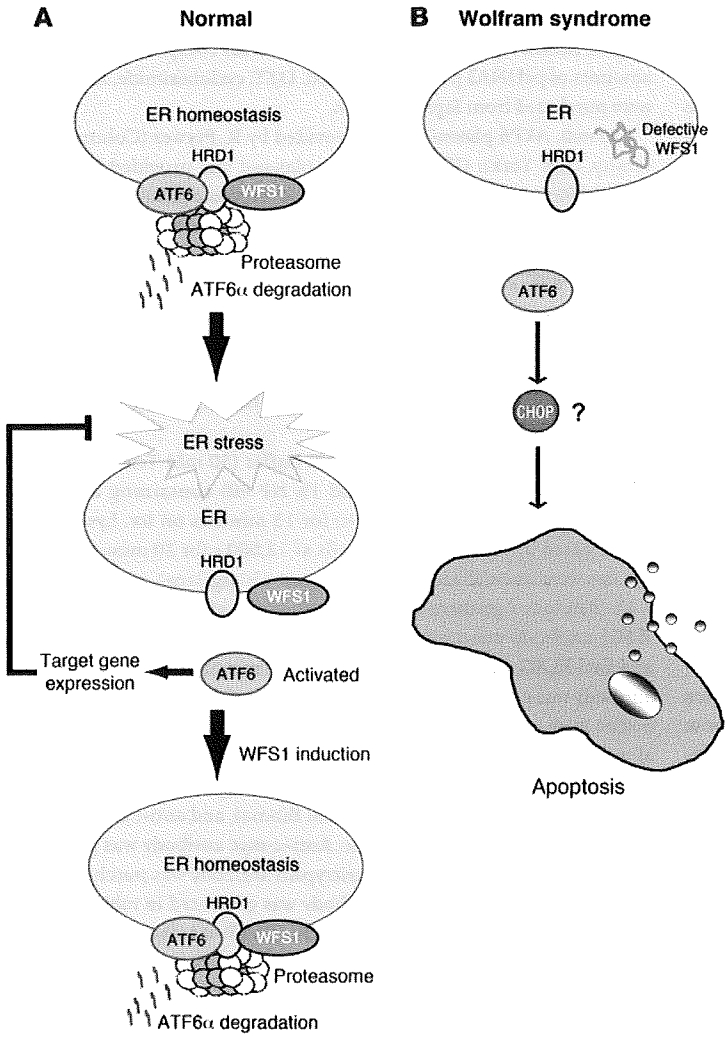

Figure 7
WFS1 controls steady-state levels of ATF6α protein and activation. (**A**) In normal cells, WFS1 recruits the ER transcription factor ATF6α to the E3 ligase Hrd1 under non–ER stress conditions. Hrd1 marks ATF6α with ubiquitin for proteasomal degradation. Under ER stress, ATF6α dissociates from WFS1 and undergoes proteolysis, and its soluble aminoportion, p60ATF6α, translocates to the nucleus, where it upregulates ER stress target genes, such as BiP, CHOP, and XBP-1. At later time points, WFS1 is induced by ER stress, which causes the eventual degradation of ATF6α. (**B**) In patients with Wolfram syndrome or *Wfs1*$^{-/-}$ mice, ATF6α escapes from the proteasome-dependent degradation, leading to chronic hyperactivation of ATF6α signaling. This ATF6α hyperactivation is involved in apoptosis through apoptotic effectors of the UPR, such as CHOP.

of the UPR, more specifically hyperactivation of ATF6α signaling, has a negative effect on β cell survival. It has been suggested that the UPR regulates both adaptive and apoptotic effectors (2, 33). The balance between these effectors depends on the nature of the ER stress, whether it is tolerable or unresolvable. Thus, the UPR acts as a binary switch between life and death. Our results demonstrated that, in patients with Wolfram syndrome and *Wfs1*$^{-/-}$ mice, unresolvable ER stress occurs in β cells and neurons, leading to a switch toward apoptosis.

ER stress is caused by both physiological and pathological stimuli that can lead to the accumulation of unfolded and misfolded proteins in the ER. Physiological ER stress can be caused by a large biosynthetic load placed on the ER, for example, during postprandial stimulation of proinsulin biosynthesis in pancreatic β cells. This stimulation leads to the activation of ER stress signaling and enhancement of insulin synthesis (34). Under physiological ER stress conditions, activation of ER stress signaling must be tightly regulated because hyperactivation or chronic activation of this signaling pathway can cause cell death. For example, when eukaryotic translation initiation factor 2α, a downstream component of ER stress signaling, is hyperphosphorylated by the compound salubrinal in pancreatic β cells, apoptosis is induced in these cells (35). Our results showed that WFS1 has an important function in the tight regulation of ER stress signaling through its interaction with a key transcription factor, ATF6α, thereby protecting cells from the damaging effects of hyperactivation of this signaling pathway.

On the basis of our present results, we believe WFS1 plays a similar role in mammals as HRD3 does in yeast: stabilizing and enhancing the activity of a key ER-resident E3 ligase, HRD1 (28). Thus, a loss of functional WFS1 may affect ER stress levels in 2 ways: (a) enhancing ATF6α signaling by increasing the pool of ATF6α, and (b) destabilizing HRD1 protein and thus its activity. The latter would independently contribute to ER stress by promoting the buildup of unfolded and misfolded proteins in the ER. In support of this is our present finding that silencing of HRD1 in β cell lines indeed led to mild ER stress (Supplemental Figure 16). It has previously been shown that HRD1 is regulated by the IRE1–XBP-1 pathway (26) and is activated at a later time point during ER stress. The ATF6α pathway, however, is activated at an earlier phase (36). Thus, WFS1 may also function as a switch from the ATF6α pathway to the IRE1–XBP-1 pathway, through the stabilization of HRD1 and consequent destruction of ATF6α protein. A previous publication has reported that WFS1 deficiency could lead to increased HRD1 expression (17), contrary to our findings. This discrepancy could be attributed to the fact that WFS1 deficiency can cause dysregulated ER stress signaling and can lead to hyperactivation of the IRE1–XBP-1 pathway under some circumstances.

It has been established that WFS1 is induced under ER stress (11). However, WFS1 increased steadily over a 24-hour time period (data not shown). ATF6α upregulation, on the other hand, occurred much more rapidly. Thus, the initial pool of WFS1 protein induced under stress may not have an inhibitory effect on ATF6α protein. In addition, we have shown that the ER-resident chaperone BiP also bound to ATF6α. The release of BiP from ATF6α when unfolded/misfolded proteins accumulate in the ER may be a key step in how ATF6α escapes WFS1-mediated proteolysis. BiP binding may be essential for the interaction of ATF6α and WFS1, and, upon release, cause a conformational change in ATF6α, leading to its consequent release from WFS1.

WFS1 is highly expressed in pancreatic β cells that are specialized for the production and regulated secretion of insulin to control blood glucose levels. In β cells, ER stress signaling needs to be tightly regulated to adapt to the frequent fluctuations of blood glucose

levels and to produce the proper amount of insulin in response to the need for it (34, 37). To achieve tight regulation, mammals may have developed WFS1 as a regulator of HRD1 function in addition to SEL1. Higher expression of WFS1 in β cells, therefore, prevents hyperactivation of ER stress signaling in these cells that are particularly sensitive to disruption of ER homeostasis and dysregulation of the UPR. Therefore, WFS1 has a role in protecting β cells from death by acting as an ER stress signaling suppressor.

Mutations in the gene encoding WFS1 cause Wolfram syndrome, a genetic form of diabetes and neurodegeneration. It has been proposed that a high level of ER stress causes β cell death and neurodegeneration in this disorder. Collectively, our results suggest that a loss-of-function mutation of WFS1 causes the instability of an E3 ligase, HRD1, leading to the upregulation of ATF6α protein and hyperactivation of ATF6α signaling. Therefore, we predict that a loss-of-function or hypomorphic mutation of the WFS1, HRD1, or ATF6α genes can cause ER stress–related disorders, such as diabetes, neurodegeneration, and bipolar disorder. Indeed, it has been shown recently that common variants in WFS1 confer risk of type 2 diabetes (14–16), and there is a link between WFS1 mutations and type 1A diabetes (38, 39). It has also been shown that ATF6α polymorphisms and haplotypes are associated with impaired glucose homeostasis and type 2 diabetes (40). Excessive β cell loss is a component of both type 1 and type 2 diabetes (41); therefore, WFS1 may have a key role in the protection of these cells from apoptosis through the tight regulation of ER stress signaling, thereby suppressing the diabetes phenotype. In addition, about 60% of patients with Wolfram syndrome have some mental disturbance such as severe depression, psychosis, or organic brain syndrome, as well as impulsive verbal and physical aggression (42). The heterozygotes who do not have Wolfram syndrome are 26-fold more likely than noncarriers to have a psychiatric hospitalization (43). The relative risk of psychiatric hospitalization for depression was estimated to be 7.1 in these heterozygotes (44). Therefore, it is possible that dysregulation of a negative feedback loop of ER stress signaling may have a pathological role in psychiatric illness.

In this study, we focused on determining the physiological function of WFS1 in ER stress signaling because of its implication in diabetes, neurodegeneration, and bipolar disorder. We propose that WFS1 has a critical function in the regulation of ER stress signaling and prevents secretory cells, such as pancreatic β cells, from dysfunction and premature death caused by hyperactivation of ER stress signaling through its interaction with the transcription factor ATF6α. WFS1 could therefore be a key target for prevention and/or therapy of ER stress–mediated diseases such as diabetes, neurodegenerative diseases, and bipolar disorder.

Methods

Cell culture. Rat insulinoma cells (INS1 832/13) were a gift from C. Newgard (Duke University Medical Center, Durham, North Carolina) and cultured in RPMI 1640 supplemented with 10% FBS. Mouse insulinoma cells (MIN6) were maintained in DMEM with 15% FBS and 1% sodium pyruvate. COS7 and Neuro2A cells were cultured in DMEM supplemented with 10% FBS. For generation of cells inducibly overexpressing WFS1 and GFP, INS-1 832/13 cells stably expressing pTetR were transduced with a lentivirus expressing human WFS1-FLAG or GFP and cultured in 2 μM doxycycline for 24 hours prior to protein/RNA isolation. For generation of cells stably suppressing WFS1 or GFP, MIN6 cells were transduced with a retrovirus expressing shRNA against mouse WFS1 or GFP. For overexpression of ATF6, Hrd1, and WFS1, COS7 cells were transfected with ATF6-HA and WFS1-FLAG expression plasmids using FuGENE 6 transfection reagent (Roche Applied Science). As a control for coexpression, equivalent amounts of pcDNA3 plasmid was used. DTT, cycloheximide, and MG132 were purchased from Sigma-Aldrich.

Plasmids. ATF6 plasmids were provided by R. Prywes (Columbia University, New York). GRP78 reporter plasmid was provided by K. Mori (Kyoto University, Japan). Hrd1-myc plasmid was a gift from M. Kaneko and M. Nomura (Hokkaido University, Sapporo, Japan). TCRα plasmids were provided by R. Kopito (Stanford University, California), and NHK3 plasmids were a gift from K. Nagata (Kyoto University). Entry vectors, destination vectors, and viral plasmids for establishing lentiviral and retroviral cell lines were provided by E. Campeau (University of Massachusetts Medical School; ref. 45). shRNA against WFS1 and GFP were purchased from the shRNA Library Core Facility at the University of Massachusetts Medical School.

IB. Cells were lysed in ice-cold TNE buffer (50 mM Tris HCl, pH 7.5; 150 mM NaCl; 1 mM EDTA; and 1% NP-40) containing a protease inhibitor cocktail (Sigma-Aldrich) for 15 minutes on ice. Lysates were then cleared by centrifuging the cells at 12,000 *g* for 20 minutes at 4°C. Lysates were normalized for total protein (30 μg/lane), separated using a 4%–20% linear gradient SDS-PAGE (BioRad), and electroblotted. Anti-WFS1 antibody was a gift from Y. Oka (Tohoku University). Anti-actin and anti-FLAG antibodies were purchased from Sigma-Aldrich. Anti-HA antibody was purchase from Stressgen, and anti-ATF6 and anti-GFP antibodies were purchased from Santa Cruz Biotechnology. Antigen retrieval was used for the anti-ATF6 antibody. Anti-ubiquitin and anti-IRE1 antibodies were purchased from Cell Signaling. Anti-alpha 5 20s proteasome antibody was purchased from Biomol, and anti-PERK antibody was purchased from Rockland Inc. Anti-c-myc antibody was purchased from Roche. The anti-alpha-1-antitrypsin antibody was purchased from DakoCytomation. Anti-Hrd1 antibody was generated in rabbits using a KLH-conjugated synthetic peptide, TCRMDVLRASLPAQS. The antibody specificity was tested by peptide/antigen competition.

DTT chase. INS-1 832/13 cells were treated with 1 mM DTT for 2 hours. The DTT was washed out with normal media (RPMI 1640 supplemented with 10% FBS) for 0, 1, or 2 hours. Cells were lysed and subjected to IP with anti-WFS1 antibodies.

Fractionation. The ER was isolated from INS-1 832/13 cells using an Endoplasmic Reticulum Isolation kit (Sigma-Aldrich). The ER pellet was then lysed in ice-cold TNE buffer containing 1% NP-40 and protease inhibitors, and the lysates were cleared and normalized. The ER lysates (1.0 ml) were loaded on top of a glycerol gradient (10%–40%) prepared in PBS containing 1 mM DTT and 2 mM ATP and centrifuged at 4°C and 80,000 *g* for 20 hours. We collected 32 fractions from the top of the tubes. Of each fraction, 200 μl was precipitated with acetone, and the remaining pellet was lysed with 50 μl sample buffer. Precipitated proteins were then separated using a 4%–20% linear gradient SDS-PAGE and electroblotted.

IP. Cells were lysed in ice-cold TNE buffer with protease inhibitors for 15 minutes on ice; the lysates were then cleared by centrifuging the cells at 12,000 *g* for 20 minutes at 4°C. For IP of endogenous WFS1, 500 μg whole cell extract from each sample was incubated with Protein G Sepharose 4 Fast Flow beads (GE Healthcare) and 4 μg anti-WFS1 antibody overnight at 4°C with rotation. After incubation, the beads were washed 3 times with TNE buffer followed by a final wash in 1× PBS. The IPs were resolved by SDS-PAGE and then subjected to IB. For IP of ATF6, 6 μg anti-ATF6 antibody was used; for HA, 2 μg anti-HA antibody was used; and for Hrd1, 4 μg anti-Hrd1 antibody was used. As a control, lysates were subjected to IP as described above using rabbit IgG.

Real-time PCR. Total RNA was isolated from the cells using the RNeasy Mini Kit (Qiagen) and reverse transcribed using 1 μg total RNA from

cells with Oligo-dT primer. For the thermal cycle reaction, the iQ5 system (BioRad) was used at 95°C for 10 minutes, then 40 cycles at 95°C for 10 seconds, and 55°C for 30 seconds. The relative amount for each transcript was calculated by a standard curve of cycle thresholds for serial dilutions of cDNA sample and normalized to the amount of actin. PCR was performed in triplicate for each sample; all experiments were repeated 3 times. The following sets of primers and Power SYBR Green PCR Master Mix (Applied Biosystems) were used for real-time PCR: rat actin, GCAAATGCTTCTAGGCGGAC and AAGAAAGGGTGTAAAACGCAGC; rat BiP, TGGGTACATTTGATCTGACTGGA and CTCAAAGGTGACTTCAATCTGGG; rat Chop, AGAGTGGTCAGTGCGCAGC and CTCATTCTCCTGCTCCTTCTCC; rat total XBP-1, TGGCCGGGTCTGCTGAGTCCG and ATCCATGGGAAGATGTTCTGG; rat ERO1-α, GAGAAGCTGTAATAGCCACGAGG and GAGCCTTTCAATAAGCGGACTG; rat GLUT2, GTGTGAGGATGAGCTGCCTAAA and TTCGAGTTAAGAGGGAGCGC; rat INS2, ATCCTCTGGGAGCCCCGC and AGAGAGCTTCCACCAAG.

Luciferase assay. COS7 cells were mock transfected, transfected with full-length ATF6 or ΔATF6 with pcDNA3.0, or transfected with ATF6 with WFS1 expression plasmids along with rat GRP78 (ERSE) promoter luciferase reporter gene, WT ATF6 binding site luciferase reporter gene (ATF6GL3), or mutant ATF6 binding site luciferase reporter gene (ATF6m1GL3) using Lipofectamine 2000 (Invitrogen). At 48 hours after transfection, lysates were prepared using a Luciferase Assay System kit (Promega). The light produced from the samples was read by a standard plate reading luminometer. Each sample was read in triplicate and normalized against the signal produced from mock wells. All experiments were repeated 3 times.

Wfs1$^{-/-}$ *animals.* *Wfs1*$^{-/-}$ mice were provided by M.A. Permutt (Washington University, St. Louis, Missouri). All procedures were reviewed and approved by the University of Massachusetts Medical School IACUC (assurance no. A-3306-01).

Statistics. To determine whether the treatment was significantly different from the control, 2-tailed paired Student's *t* test was used. A *P* value less than 0.01 was considered statistically significant. In the figures, numbers below the lanes of blots denote relative protein amounts, as quantified by ImageJ software, normalized to the respective control. All graphical data are shown as mean ± SD.

Acknowledgments

We thank Keiji Tanaka, Hideki Yashiroda, Reid Gilmore, Sara Evans, and Michael R. Green for comments on the manuscript; Julie Zhu for statistical analysis; Karen Sargent, Jessica Crisci, Yuan Lee, Linda Leehy, and Cris Welling for technical assistance; and Carlos Fonseca for support and advice. This work was supported by grants from NIDDK, NIH (R01 DK067493), the Diabetes and Endocrinology Research Center at the University of Massachusetts Medical School (5 P30 DK32520), the Juvenile Diabetes Research Foundation International, the Worcester Foundation for Biomedical Research, and the Iacocca Foundation to F. Urano.

Received for publication April 27, 2009, and accepted in revised form January 6, 2010.

Address correspondence to: Fumihiko Urano, Program in Gene Function and Expression, University of Massachusetts Medical School, Worcester, MA 01605-2324. Phone: 508.856.6012; Fax: 508.856.4650; E-mail: Fumihiko.Urano@umassmed.edu.

1. Ron D, Walter P. Signal integration in the endoplasmic reticulum unfolded protein response. *Nat Rev Mol Cell Biol.* 2007;8(7):519–529.
2. Rutkowski DT, Kaufman RJ. That which does not kill me makes me stronger: adapting to chronic ER stress. *Trends Biochem Sci.* 2007;32(10):469–476.
3. Haze K, Yoshida H, Yanagi H, Yura T, Mori K. Mammalian transcription factor ATF6 is synthesized as a transmembrane protein and activated by proteolysis in response to endoplasmic reticulum stress. *Mol Biol Cell.* 1999;10(11):3787–3799.
4. Yoshida H, et al. ATF6 activated by proteolysis binds in the presence of NF-Y (CBF) directly to the cis-acting element responsible for the mammalian unfolded protein response. *Mol Cell Biol.* 2000; 20(18):6755–6767.
5. Ye J, et al. ER stress induces cleavage of membrane-bound ATF6 by the same proteases that process SREBPs. *Mol Cell.* 2000;6(6):1355–1364.
6. Shen J, Chen X, Hendershot L, Prywes R. ER stress regulation of ATF6 localization by dissociation of BiP/GRP78 binding and unmasking of Golgi localization signals. *Dev Cell.* 2002;3(1):99–111.
7. Wu J, et al. ATF6alpha optimizes long-term endoplasmic reticulum function to protect cells from chronic stress. *Dev Cell.* 2007;13(3):351–364.
8. Yamamoto K, et al. Transcriptional induction of mammalian ER quality control proteins is mediated by single or combined action of ATF6alpha and XBP1. *Dev Cell.* 2007;13(3):365–376.
9. Hong M, Li M, Mao C, Lee AS. Endoplasmic reticulum stress triggers an acute proteasome-dependent degradation of ATF6. *J Cell Biochem.* 2004; 92(4):723–732.
10. Takeda K, et al. WFS1 (Wolfram syndrome 1) gene product: predominant subcellular localization to endoplasmic reticulum in cultured cells and neuronal expression in rat brain. *Hum Mol Genet.* 2001; 10(5):477–484.
11. Fonseca SG, et al. WFS1 is a novel component of the unfolded protein response and maintains homeostasis of the endoplasmic reticulum in pancreatic {beta}-cells. *J Biol Chem.* 2005;280(47):39609–39615.
12. Strom TM, et al. Diabetes insipidus, diabetes mellitus, optic atrophy and deafness (DIDMOAD) caused by mutations in a novel gene (wolframin) coding for a predicted transmembrane protein. *Hum Mol Genet.* 1998;7(13):2021–2028.
13. Inoue H, et al. A gene encoding a transmembrane protein is mutated in patients with diabetes mellitus and optic atrophy (Wolfram syndrome). *Nat Genet.* 1998;20(2):143–148.
14. Lyssenko V, et al. Clinical risk factors, DNA variants, and the development of type 2 diabetes. *N Engl J Med.* 2008;359(21):2220–2232.
15. Franks PW, et al. Replication of the association between variants in WFS1 and risk of type 2 diabetes in European populations. *Diabetologia.* 2008; 51(3):458–463.
16. Sandhu MS, et al. Common variants in WFS1 confer risk of type 2 diabetes. *Nat Genet.* 2007;39(8):951–953.
17. Yamada T, et al. WFS1-deficiency increases endoplasmic reticulum stress, impairs cell cycle progression and triggers the apoptotic pathway specifically in pancreatic beta-cells. *Hum Mol Genet.* 2006;15(10):1600–1609.
18. Riggs AC, et al. Mice conditionally lacking the Wolfram gene in pancreatic islet beta cells exhibit diabetes as a result of enhanced endoplasmic reticulum stress and apoptosis. *Diabetologia.* 2005;48(11):2313–2321.
19. Kakiuchi C, Ishiwata M, Hayashi A, Kato T. XBP1 induces WFS1 through an endoplasmic reticulum stress response element-like motif in SH-SY5Y cells. *J Neurochem.* 2006;97(2):545–555.
20. Wang Y, Shen J, Arenzana N, Tirasophon W, Kaufman RJ, Prywes R. Activation of ATF6 and an ATF6 DNA binding site by the endoplasmic reticulum stress response. *J Biol Chem.* 2000;275(35):27013–27020.
21. Shen J, Snapp EL, Lippincott-Schwartz J, Prywes R. Stable binding of ATF6 to BiP in the endoplasmic reticulum stress response. *Mol Cell Biol.* 2005; 25(3):921–932.
22. Yu H, Kaung G, Kobayashi S, Kopito RR. Cytosolic degradation of T-cell receptor alpha chains by the proteasome. *J Biol Chem.* 1997;272(33):20800–20804.
23. Yu H, Kopito RR. The role of multiubiquitination in dislocation and degradation of the alpha subunit of the T cell antigen receptor. *J Biol Chem.* 1999; 274(52):36852–36858.
24. Hosokawa N, et al. A novel ER alpha-mannosidase-like protein accelerates ER-associated degradation. *EMBO Rep.* 2001;2(5):415–422.
25. Kaneko M, et al. A different pathway in the endoplasmic reticulum stress-induced expression of human HRD1 and SEL1 genes. *FEBS Lett.* 2007; 581(28):5355–5360.
26. Yamamoto K, et al. Human HRD1 promoter carries a functional unfolded protein response element to which XBP1 but not ATF6 directly binds. *J Biochem.* 2008;144(4):477–486.
27. Hampton RY, Gardner RG, Rine J. Role of 26S proteasome and HRD genes in the degradation of 3-hydroxy-3-methylglutaryl-CoA reductase, an integral endoplasmic reticulum membrane protein. *Mol Biol Cell.* 1996;7(12):2029–2044.
28. Gardner RG, et al. Endoplasmic reticulum degradation requires lumen to cytosol signaling. Transmembrane control of Hrd1p by Hrd3p. *J Cell Biol.* 2000;151(1):69–82.
29. Ishihara H, et al. Disruption of the WFS1 gene in mice causes progressive beta-cell loss and impaired stimulus-secretion coupling in insulin secretion. *Hum Mol Genet.* 2004;13(11):1159–1170.
30. Kudo T, et al. A molecular chaperone inducer protects neurons from ER stress. *Cell Death Differ.* 2008;15(2):364–375.
31. Martindale JJ, et al. Endoplasmic reticulum stress gene induction and protection from ischemia/reperfusion injury in the hearts of transgenic mice with a tamoxifen-regulated form of ATF6. *Circ Res.* 2006; 98(9):1186–1193.
32. Ye R, et al. Grp78 heterozygosity promotes adap-

tive unfolded protein response and attenuates diet-induced obesity and insulin resistance. *Diabetes.* 2010; 59(1):6–16.
33. Han D, et al. IRE1alpha kinase activation modes control alternate endoribonuclease outputs to determine divergent cell fates. *Cell.* 2009;138(3):562–575.
34. Lipson KL, et al. Regulation of insulin biosynthesis in pancreatic beta cells by an endoplasmic reticulum-resident protein kinase IRE1. *Cell Metab.* 2006; 4(3):245–254.
35. Cnop M, et al. Selective inhibition of eukaryotic translation initiation factor 2 alpha dephosphorylation potentiates fatty acid-induced endoplasmic reticulum stress and causes pancreatic beta-cell dysfunction and apoptosis. *J Biol Chem.* 2007;282(6):3989–3997.
36. Yoshida H, Matsui T, Hosokawa N, Kaufman RJ, Nagata K, Mori K. A time-dependent phase shift in the mammalian unfolded protein response. *Dev Cell.* 2003;4(2):265–271.
37. Fonseca SG, Lipson KL, Urano F. Endoplasmic reticulum stress signaling in pancreatic beta-cells. *Antioxid Redox Signal.* 2007;9(12):2335–2344.
38. Nakamura A, et al. A novel mutation of WFS1 gene in a Japanese man of Wolfram syndrome with positive diabetes-related antibodies. *Diabetes Res Clin Pract.* 2006;73(2):215–217.
39. Awata T, et al. Missense variations of the gene responsible for Wolfram syndrome (WFS1/wolframin) in Japanese: possible contribution of the Arg456His mutation to type 1 diabetes as a nonautoimmune genetic basis. *Biochem Biophys Res Commun.* 2000;268(2):612–616.
40. Meex SJ, et al. Activating transcription factor 6 polymorphisms and haplotypes are associated with impaired glucose homeostasis and type 2 diabetes in Dutch Caucasians. *J Clin Endocrinol Metab.* 2007;92(7):2720–2725.
41. Butler AE, Janson J, Bonner-Weir S, Ritzel R, Rizza RA, Butler PC. Beta-cell deficit and increased beta-cell apoptosis in humans with type 2 diabetes. *Diabetes.* 2003;52(1):102–110.
42. Swift RG, Sadler DB, Swift M. Psychiatric findings in Wolfram syndrome homozygotes. *Lancet.* 1990;336(8716):667–669.
43. Swift RG, Polymeropoulos MH, Torres R, Swift M. Predisposition of Wolfram syndrome heterozygotes to psychiatric illness. *Mol Psychiatry.* 1998;3(1):86–91.
44. Swift M, Swift RG. Wolframin mutations and hospitalization for psychiatric illness. *Mol Psychiatry.* 2005;10(8):799–803.
45. Campeau E, et al. A versatile viral system for expression and depletion of proteins in mammalian cells. *PLoS ONE.* 2009;4(8):e6529.

Psychiatry and Clinical Neurosciences 2009; 63: 65–72 doi:10.1111/j.1440-1819.2008.01889.x

Regular Article

Neuropathy is associated with depression independently of health-related quality of life in Japanese patients with diabetes

Sumiko Yoshida, MD, PhD,[1]* Masashi Hirai, MD, PhD,[2] Susumu Suzuki, MD, PhD,[2] Shuichi Awata, MD, PhD[3] and Yoshitomo Oka, MD, PhD[2]

[1]*Department Psychiatry, Faculty of Medicine, Saitama Medical University, Saitama,* [2]*Division of Molecular Metabolism and Diabetes, Tohoku University Graduate School of Medicine, and* [3]*Department of Psychiatry, Tohoku University Graduate School of Medicine, Sendai, Japan*

Objectives: To identify factors independently associated with depression in Japanese patients with diabetes, after controlling for potential confounding factors.

Methods: Among 197 outpatients with diabetes, 129 (type 1: 24, type 2: 105) completed a questionnaire concerning socio-demographic and health-related variables. Depression screening was done using Zung's Self-Rating Depression Scale test, followed by diagnostic interviews by experienced psychiatrists employing the Diagnostic Statistical Manual of Mental Disorders, 4th edition (DSM-IV).

Results: Forty-seven patients (36.4%) had symptomatological depression. A Self-Rating Depression Scale cut-off score of 40 had good sensitivity (100%) and modest specificity (59%) for detecting major depressive episode, in accordance with the DSM-IV. Diabetic patients suffering from depression were more likely to have neuropathy, retinopathy, body pain, a feeling of poor general health, and lack of social support, than the non-depressed patients. However, age, gender, marital status, diabetes type, insulin requirement, duration of diabetes, hemoglobin A1c (HbA1c) and the presence of nephropathy did not differ between the two groups. In multivariate logistic regression analysis, body pain (OR 3.26, 95% CI 1.31–8.08) and the presence of microvascular complications (OR 2.81, 95% CI 1.13–6.98) were independent factors associated with depression. Specifically, diabetic neuropathy (OR 3.10, 95% CI 1.17–8.22) was associated with depression independently of age, gender, marital status, social supports, quality of life, diabetes type, duration of diabetes, HbA1c, and insulin requirement.

Conclusions: A diabetic complication, specifically neuropathy, was independently associated with depression in patients with diabetes. The present findings indicate the need to find a biological base common to both depression in diabetes and diabetic neuropathy.

Key words: depression, diabetes, mental health, neuropathy, quality of life

DEPRESSION IS MORE common among diabetic patients in western countries. Recent studies have documented a doubling of depression rates in individuals with, as compared to those without, diabetes.[1,2] It has been shown that diabetic patients who are depressed have poorer glycemic control,[3] are less physically active,[4] and more obese.[5] Depression appears to be a very important problem in the management of diabetes.

**Correspondence: Sumiko Yoshida, MD, PhD, Deptartment Psychiatry, Faculty of Medicine, Saitama Medical University, Moroyama-machi, Iruma, Saitama 350-0495, Japan. Email: yoshidas@saitama-med.ac.jp*

Address of the institution at which the work was carried out: Div. Molecular Metabolism and Diabetes, Tohoku Univ. Grad. Sch. Med., Sendai, 980-8575, Japan

Received 11 February 2008; revised 13 September 2008; accepted 14 September 2008.

To date, the socio-demographic factors reported to be associated with depression include: female gender,[2] younger age,[2,6] being unmarried,[2,7,8] lower levels of education[6,8] and lack of social support.[9] Factors concerning health-related quality of life (QOL), such as perception of poor general health[10] and body pain,[11] were also associated with depression. Poor glycemic control,[3,7] types of diabetes treatment,[8] duration of diabetes,[8] presence of diabetic complications,[8,12] diabetic neuropathy[13–15] and retinopathy[9,16] were similarly associated with depression. However, these reports did not adequately control for potential confounding factors. Are there any factors underlying both depression and diabetes?

The prevalence of major depressive episodes in the Japanese diabetic population according to the Diagnostic Statistical Manual of Mental Disorders 4th edition (DSM-IV),[17] has not been investigated. In addition, only a few studies designed to identify factors associated with depression in individuals with diabetes in Asian countries, including Japan, have been reported. We first investigated the prevalence of depression, diagnosed by experienced psychiatrists, to confirm the increased prevalence of major depressive episodes in Japanese diabetic patients. Then we investigated factors possibly associated with depression in diabetic patients using multivariate logistic analysis, after controlling for the potential confounding factors.

METHODS

Subjects

All 197 patients who visited the Diabetes and Metabolism Unit, Tohoku University Hospital in November 2003 were recruited. The diagnosis of type 1 or type 2 diabetes had been made in accordance with the criteria of the American Diabetes Association.[18] One hundred twenty-nine of the 197 patients (65%) completed a questionnaire concerning socio-demographic and health-related variables. This study was conducted under the guidelines of the ethics committee at the Tohoku University. The procedures were fully explained to each subject before the assessments and written informed consent was obtained from each subject.

Measurement

Gender, age, marital status, the number of family members, educational level, and social support were assessed as socio-demographic variables. For social support, one item was selected from among the five items used in previous Japanese studies[19,20] as the strongest association with depression was found in the present samples. Health-related quality of life was assessed using the subscales for pain and perception of general health in the Japanese version of the Short-Form 36 Health Survey questionnaire.[21,22] All scores were dichotomized by the average score of the Japanese general population.

Diabetes type (Types 1 and 2), duration of illness (≧10 and <10 years), body mass index (BMI), medical regimen, anti-hypertensive requirements, hypolipidemic requirements, and blood pressure were obtained from the patient's medical record. Fasting plasma glucose concentration, hemoglobin A1c (HbA1c, ≧7 and <7%), and plasma lipid levels (Triglycerides [TG], total cholesterol [TC], high density lipoprotein cholesterol [HDL], and low density lipoprotein cholesterol [LDL]) were also evaluated as variables representing glycemic control status.

Microvascular complications were defined as the presence of at least one of the following: diabetic nephropathy, neuropathy or retinopathy. Diabetic nephropathy was defined as the presence of persistent proteinuria. Diabetic neuropathy was defined as the presence of symmetric neuropathic symptoms in the lower extremities and/or absence of bilateral Achilles tendon reflexes. Diabetic retinopathy, diagnosed by experienced ophthalmologists, was categorized as: simple, preproliferative or proliferative retinopathy, or none.

Assessment of depression

The Zung Self-Rating Depression Scale (SDS)[23] was used to screen for depression. Patients scoring 40 or more on the SDS were defined as suffering from depression.[24,25] The Japanese version of the SDS has been extensively validated.[26] All patients with a score of 40 or more on the SDS were suggested to undergo a psychiatric evaluation using the DSM-IV to diagnose a possible major depressive episode within the following one-month period. Almost the same number of patients with scores under 40 on the SDS had the same interviews as the controls. None of the subjects who were interviewed were taking any psychoactive drugs during the study.

Statistical analysis

The χ^2 test or *t*-test was used to compare differences in characteristics between diabetic patients with and without depression. Multivariate logistic regression analysis was used to estimate the association between depression and potential predictor variables by calculating odds ratios (OR) and 95% confidence intervals (95% CI). All statistical analyses were performed using SPSS for Windows, version 11.5J. A value of $P < 0.05$ was considered to be statistically significant.

RESULTS

Prevalence of depression and major depressive episode

Forty- seven out of 129 subjects (36.4%) had depression. Thirty-one of the 47 depressed subjects underwent diagnostic interviewing by experienced psychiatrists. Seven (type 1: 3, type 2: 4) of these 31 were diagnosed as having a major depressive episode. None of 34 subjects with SDS scores below 40, who had the same interviews, were diagnosed as having a major depressive episode. (Fig. 1 shows the experimental design.) Thus, the prevalence of a current major depressive episode in adult diabetic patients was estimated to be 7.9%. There is no difference of the prevalence between type 1 and type 2 ($P = 0.34$). In this study, an SDS cut-off of 40 yielded good sensitivity (100%) and modest specificity (59%) for detecting a major depressive episode in accordance with the DSM-IV.

Comparison of characteristics of diabetic patients with and without depression

The characteristics of patients with and without depression are presented in Table 1. The depressed

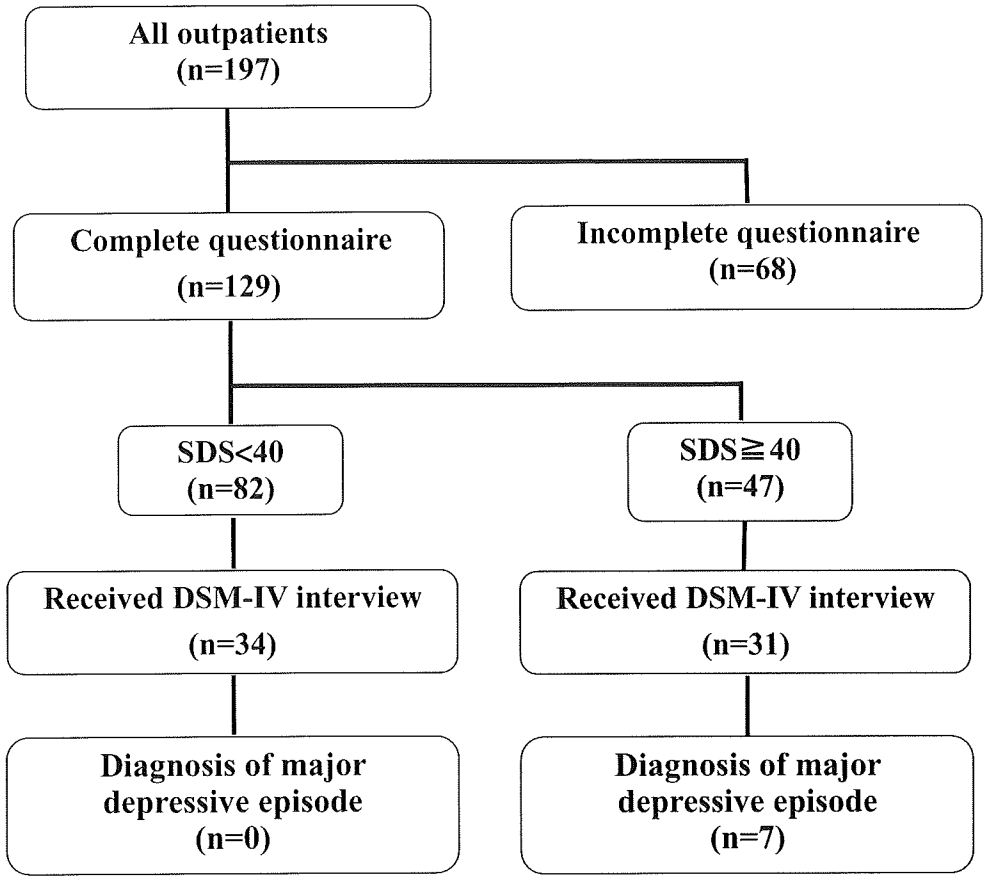

Figure 1. Experimental design. SDS, Zung Self-Rating Depression Scale; DSM-IV, Diagnostic Statistical Manual of Mental Disorders, 4th edition.

Table 1. Characteristics of patients with and without depression

Variables	SDS < 40 ($n = 82$)	SDS ≧ 40 ($n = 47$)
Gender		
Female	35	23
Male	47	24
Age	54.12 ± 10.31	52.72 ± 10.47
Martial status		
Married	66	32
Unmarried	16	15
Number of family members	3.13 ± 1.45	3.32 ± 1.80
Social support		
+	77	38
−	5	9*
SF36: pain	76.72 ± 23.80	63.24 ± 27.00**
SF36: general health	54.82 ± 18.00	40.93 ± 22.91**
Education		
~ junior high school	9	4
~ high school	42	33
~ college (university)	31	10
Diabetes type		
Type 1	13	11
Type 2	69	36
Duration of illness		
<10 years	53	24
≧10 years	29	23
BMI (kg/M^2)	24.07 ± 4.69	24.07 ± 3.74
Insulin		
+	45	27
−	37	20
Anti-hypertensive agent		
+	25	12
−	57	35
Hypolipidemic agent		
+	27	9
−	55	38
Blood pressure (mmHg)	127.6 ± 15.0	126.3 ± 15.8
Diastolic	77.4 ± 10.1	75.0 ± 8.8
Systolic	146.61 ± 38.20	154.04 ± 66.90
Fasting blood glucose (mg/dl)	7.00 ± 1.19	7.12 ± 1.69
HbA1c (%)	112.76 ± 59.93	118.57 ± 73.70
TG (mg/dl)	193.82 ± 28.90	193.60 ± 35.99
TC (mg/dl)	56.40 ± 19.84	52.60 ± 17.25
HDL (mg/dl)	113.57 ± 26.10	117.40 ± 30.83
LDL (mg/dl)		
Microvascular complications		
+	28	28**
−	54	19
Nephropathy		
+	12	5
−	70	42
Neuropathy		
+	14	18**
−	68	29
Retinopathy		
+	19	20*
−	63	27

Data are means ± SD or N. BMI, body mass index; HbA1c, hemoglobin A1c; HDL, high density lipoprotein cholesterol; LDL, low density lipoprotein cholesterol; SDS, Zung Self-Rating Depression Scale; SF36, Short-Form 36 Health Survey questionnaires, TC, total cholesterol; TG, triglycerides; persons without pain have higher pain scores, persons who perceive themselves as having good health have higher scores for general health. *$P < 0.05$; **$P < 0.01$ by t-test or χ^2 test.

patients were more likely to lack social support ($P < 0.05$), have pain (P. 0.01), and feel that their general health was poor ($P < 0.01$), than patients without depression. The prevalence of microvascular complications, that is, diabetic neuropathy and/or retinopathy, was also higher in the patients with than in those without depression ($P < 0.01$). In contrast, age, gender, marital status and educational level did not differ between the two groups. There was also no difference in the diabetes type, duration of diabetes, BMI, insulin requirement, blood pressure, antihypertensive medication requirement, fasting plasma glucose concentration, HbA1c, plasma lipid levels, hypolipidemic medication requirement or the presence of nephropathy between the depressed and non-depressed patients.

Multivariate analysis

Tables 2 and 3 show the factors predictably associated with depression in diabetic patients. As shown in Table 2, the subjective feeling of body pain (OR = 3.26, 95% CI = 1.31–8.08) and the presence of microvascular complications (OR = 2.81, 95% CI = 1.13–6.98) were independently associated with depression. In the analysis focused on neuropathy rather than the presence of microvascular complications in general, the presence of diabetic neuropathy (OR = 3.10, 95% CI = 1.17–8.22) was significantly associated with depression (Table 3). This association was independent of age, gender, marital status, social support, pain, a perception of poor general health, diabetes type, duration of diabetes, HbA1c, and insulin requirement. Neither nephropathy nor retinopathy was independently associated with depression.

Table 2. Factors independently associated with depression: with respect to microvascular complications

Independent variables	OR	95% CI	p
Age	0.99	0.95–1.03	0.76
Gender			
Male	1.00		
Female	1.10	0.47–2.58	0.83
Marital status			
Married	1.00		
Unmarried	1.55	0.60–4.01	0.37
Social support			
+	1.00		
–	2.04	0.68–8.55	0.17
SF 36: pain			
≧76.2	1.00		
<76.2	3.26	1.31–8.08	0.011*
SF 36: general health			
≧65.0	1.00		
<65.0	1.34	0.47–3.80	0.58
Type of diabetes			
Type 2	1.00		
Type 1	2.02	0.68–5.98	0.21
Duration of diabetes (years)			
<10	1.00		
≧10	1.75	0.74–3.92	0.21
HbA1c (%)			
<7.0	1.00		
≧7.0	0.56	0.23–1.37	0.20
Insulin			
–	1.00		
+	0.76	0.28–2.02	0.58
Microvascular complication			
–	1.00		
+	2.81	1.13–6.98	0.026*

*$P < 0.05$ by multivariate logistic regression analysis.
65.0, mean score on the general health subscale of the SF36 in the Japanese population (persons who perceive themselves as having good health have higher scores); 76.2, mean score on the pain subscale of the SF36 in the Japanese population (persons without pain have higher scores); 95% CI, 95% confidence intervals; HbA1c, hemoglobin A1c; OR, odds ratio; SF36: Short-Form 36 Health Survey questionnaire.

DISCUSSION

The prevalence of a DSM-IV major depressive episode in adult diabetic patients was estimate to be 7.9%, that is, higher than that of the general Japanese population (1%; DSM-III)[27] or working population (4%; ICD-10).[28] The prevalence range for current depression, diagnosed by structured diagnostic interviews of diabetic patients, was reported to be 11.0–19.9% in uncontrolled studies.[29] The prevalence determined in this study was lower than those reported previously. It might partially be explained by the fact that 16 out of 47 depressive patients who seemed to have severed depressive symptoms refused to be psychiatrically interviewed. However, our result confirmed an increased prevalence of a major depressive episode in diabetic patients as compared to the general population not only in Western countries but also in Japan.

Our findings on the characteristics of patients with and without depression are partially consistent with the results of earlier studies on the relationship

Table 3. Factors independently associated with depression: with respect to neuropathy

Independent variables	OR	95% CI	*P*
Age	1.00	0.95–1.04	0.83
Gender			
Male	1.00		
Female	1.04	0.45–2.43	0.93
Marital status			
Married	1.00		
Unmarried	1.74	0.67–4.51	0.26
Social support			
+	1.00		
−	2.64	0.76–9.22	0.13
SF 36: pain			
≧76.2	1.00		
<76.2	3.53	1.42–8.81	0.007**
SF 36: general health			
≧65.0	1.00		
<65.0	1.25	0.44–3.50	0.68
Type of diabetes			
Type 2	1.00		
Type 1	1.96	0.66–5.77	0.23
Duration of diabetes (years)			
≧10	1.71		
<10	1.00	0.75–3.93	0.21
HbA1c (%)			
<7.0	1.00		
≧7.0	0.57	0.23–1.41	0.22
Insulin			
−	1.00		
+	0.78	0.30–2.11	0.64
Neuropathy			
−	1.00		
+	3.10	1.17–8.22	0.023*

*$P < 0.05$; **$P < 0.01$ by multivariate logistic regression analysis.
65.0, mean score on the general health subscale of the SF36 in the Japanese population (persons who perceive themselves as having good health have higher scores); 76.2, mean score on the pain subscale of the SF36 in the Japanese population (persons without pain have higher scores); 95% CI, 95% confidence intervals; HbA1c, hemoglobin A1c; OR, odds ratio; SF36, Short-Form 36 Health Survey questionnaire.

between diabetes and depression. Relationships between lack of social support,[9] perception of poor general health[10] or body pain[11] and depression in diabetic patients have been reported previously. Similarly, the presence of microvascular complications,[8,12] specifically neuropathy[13–15] and retinopathy,[9,16] are related to depression. However, our results do not support a relationship between depression and the following factors; female gender,[2] younger age,[2,6] being unmarried,[2,7] lower levels of education,[6,8] poor glycemic control,[3,7] types of diabetes treatment[8] and duration of diabetes.[8] The discrepancies across studies might be attributable, at least in part, to differences in patient characteristics. The patients in our study had essentially adequate glycemic control (HbA1c: 7.0 ± 1.4, FBS: 149 ± 50) at the start of the study and most had attained a high level of education. Thus, glycemic control status and educational level appear not to be related to depression.

In multivariate logistic regression analysis, the presence of microvascular complications, specifically neuropathy, was associated with depression independently of age, gender, marital status, social support, pain, perception of general health, diabetes type, duration of diabetes, HbA1c, and insulin requirement. Diabetic complications decreased health-related QOL, which is associated with increased risk of psychological impairment.[30,31] One of the subscales for health-related QOL, body pain, was also reported to be strongly associated with depression.[11,13] It was also suggested that individuals with inadequate support are most at risk of becoming depressed when disability related to illness increased.[31] Thus, several previous reports suggested depression in diabetic patients to be secondarily induced by decreased health-related QOL and/or inadequate social support. However, our results demonstrate that depression is not necessarily secondarily induced by pre-existing factors because a diabetic complication, specifically neuropathy, was independently associated with depression regardless of health-related QOL and/or social support.

There is a possibility that diabetic microvascular impairment induces both neuropathy[32] and so-called vascular depression[33] in diabetic patients. However, it seems unlikely that depression in diabetic patients would be vascular in origin because neither nephropathy nor retinopathy was independently associated with depression in this study.

The present findings indicate the need to find a biological base common to both depression in diabetes and diabetic neuropathy.

However, there are limitations to interpreting the results of this study. First, because this analysis is based on cross-sectional data, causality can not be determined. Prospective studies are needed. Second, this study has sample size limitation. Future studies

enrolling adequate samples of diabetic patients are required.

CONCLUSION

Diagnostic interviews, conducted by experienced psychiatrists, demonstrated a higher prevalence of current major depressive episodes (7.9%) in Japanese diabetic patients than in the general population. Multivariate logistic regression analyses demonstrated neuropathy to be an independent factor associated with depression in diabetic patients.

ACKNOWLEDGMENTS

This work was supported by a Grant-in-Aid for Research on the Human Genome, Tissue Engineering (H17-genome-003) from the Ministry of Health, Labour and Welfare of Japan to Y. O.

REFERENCES

[1] Anderson RJ, Freedland KE, Clouse RE, Lustman PJ. The prevalence of comorbid depression in adults with diabetes: A meta-analysis. *Diabetes Care* 2001; **24**: 1069–1078.

[2] Egede LE, Zheng D, Simpson K. Comorbid depression is associated with increased health care use and expenditures in individuals with diabetes. *Diabetes Care* 2002; **25**: 464–470.

[3] Lustman PJ, Anderson RJ, Freedland KE, de Groot M, Carney RM, Clouse RE. Depression and poor glycemic control: A meta-analytic review of the literature. *Diabetes Care* 2000; **23**: 934–942.

[4] Caruso LB, Silliman RA, Demissie S, Greenfield S, Wagner EH. What can we do to improve physical function in older persons with type 2 diabetes? *J. Gerontol. A Biol. Sci. Med. Sci.* 2000; **55**: M372–M377.

[5] Katon W, von Kroff M, Ciechanowski P *et al.* Behavioral and clinical factors associated with depression among persons with diabetes. *Diabetes Care* 2004; **27**: 914–920.

[6] Peyrot M, Rubin RR. Persistence of depressive symptoms in diabetic adults. *Diabetes Care* 1999; **22**: 448–452.

[7] Hanninen JA, Takala JK, Keinanen-Kiukaanniemi SM. Depression in subjects with type 2 diabetes. Predictive factors and relation to quality of life. *Diabetes Care* 1999; **22**: 997–998.

[8] Peyrot M, Rubin RR. Levels and risks of depression and anxiety symptomatology among diabetic adults. *Diabetes Care* 1997; **20**: 585–590.

[9] Miyaoka Y, Miyaoka H, Motomiya T, Kitamura S, Asai M. Impact of sociodemographic and diabetes-related characteristics on depressive state among non-insulin-dependent diabetic patients. *Psychiatry Clin. Neurosci.* 1997; **51**: 203–206.

[10] Jacobson AM, de Groot M, Samson JA. The effects of psychiatric disorders and symptoms on quality of life in patients with type I and type II diabetes mellitus. *Qual. Life Res.* 1997; **6**: 11–20.

[11] Bair MJ, Robinson RL, Katon W, Kroenke K. Depression and pain comorbidity: A literature review. *Arch. Intern. Med.* 2003; **163**: 2433–2445.

[12] Padgett DK. Sociodemographic and disease-related correlates of depressive morbidity among diabetic patients in Zagreb, Croatia. *J. Nerv. Ment. Dis.* 1993; **181**: 123–129.

[13] Takahashi Y, Hirata Y. A follow-up study of painful diabetic neuropathy: Physical and psychological aspects. *Tohoku J. Exp. Med.* 1983; **141**: 463–471.

[14] Winocour PH, Main CJ, Medlicott G, Anderson DC. A psychometric evaluation of adult patients with type 1 (insulin-dependent) diabetes mellitus: Prevalence of psychological dysfunction and relationship to demographic variables, metabolic control and complications. *Diabetes Res.* 1990; **14**: 171–176.

[15] Viinamäki H, Niskanen L, Uusitupa M. Mental well-being in people with non-insulin-dependent diabetes. *Acta Psychiatr. Scand.* 1995; **92**: 392–397.

[16] Black SA. Increased health burden associated with comorbid depression in older diabetic Mexican Americans. Results from the Hispanic Established Population for the Epidemiologic Study of the Elderly survey. *Diabetes Care* 1999; **22**: 56–64.

[17] American Psychiatric Association. *Diagnostic and Statistical Manual of Mental Disorders*, 4th edn. American Psychiatric Association, Washington, DC, 1994.

[18] The expert committee on the diagnosis and classification of diabetes mellitus. Report of the expert committee on the diagnosis and classification of diabetes mellitus. *Diabetes Care* 1997; **20**: 1183–1197.

[19] Muraoka Y, Oiji A, Ihara K. The physical, psychological and social background factors of elderly depression in the community (in Japanese). *Jpn. J. Geriatr. Psychiatry* 1996; **7**: 397–407.

[20] Koizumi Y, Awata S, Seki T *et al.* Association between social support and depression in the elderly Japanese population (in Japanese with English abstract). *Nippon Ronen Igakkai Zasshi* 2004; **41**: 426–433.

[21] Fukuhara S, Bito S, Green J, Hsiao A, Kurokawa K. Translation, adaptation, and validation of the SF-36 Health Survey for use in Japan. *J. Clin. Epidemiol.* 1998; **51**: 1037–1044.

[22] Fukuhara S, Ware JE Jr, Kosinski M, Wada S, Gandek B. Psychometric and clinical tests of validity of the Japanese SF-36 Health Survey. *J. Clin. Epidemiol.* 1998; **51**: 1045–1053.

[23] Zung WA. Self-rating depression scale. *Arch. Gen. Psychiatry* 1965; **12**: 63–70.

[24] Zung WWK. A cross-cultural survey of symptoms in depression. *Am. J. Psychiatry* 1969; **126**: 116–121.

[25] Barrett J, Hurst MW, DiScala C, Rose RM. Prevalence of depression over a 12-month period in a non-patient population. *Arch. Gen. Psychiatry* 1978; **35**: 741–744.
[26] Fukuda K, Kobayashi S. A study on a self-rating depression scale. *Psychiatr. Neurol. Jpn.* 1978; **75**: 673–679.
[27] Fujihara S, Kitamura T. Psychiatric epidemiologic research in an area of Kofu city: The prevalence of mild psychiatric disorder using JCM diagnosis (in Japanese). *Nippon Iji Shinpou* 1992; **3618**: 47–50.
[28] Kawakami N, Iwata N, Tanigawa T *et al.* Prevalence of mood and anxiety disorders in a working population in Japan. *J. Occup. Environ. Med.* 1996; **38**: 899–905.
[29] Gavard JA, Lustman PJ, Clouse RE. Prevalence of depression in adults with diabetes. An epidemiological evaluation. *Diabetes Care* 1993; **16**: 1167–1178.
[30] Jacobson AM, Rand LI, Hauser ST. Psychologic stress and glycemic control: A comparison of patients with and without proliferative diabetic retinopathy. *Psychosom. Med.* 1985; **47**: 327–381.
[31] Littlefield CH, Rodin GM, Murray MA, Craven JL. Influence of functional impairment and social support on depressive symptoms in persons with diabetes. *Health Psychol.* 1990; **9**: 737–749.
[32] Low PA. Recent advances in the pathogenesis of diabetic neuropathy. *Muscle Nerve* 1987; **10**: 121–128.
[33] Alexopoulos GS, Meyers BS, Young RC, Campbell S, Silbersweig D, Charlson M. 'Vascular depression' hypothesis. *Arch. Gen. Psychiatry* 1997; **54**: 915–922.

DOC2B: A Novel Syntaxin-4 Binding Protein Mediating Insulin-Regulated GLUT4 Vesicle Fusion in Adipocytes

Naofumi Fukuda,[1] Masahiro Emoto,[1] Yoshitaka Nakamori,[1] Akihiko Taguchi,[1] Sachiko Miyamoto,[1] Shinsuke Uraki,[1] Yoshitomo Oka,[2] and Yukio Tanizawa[1]

OBJECTIVE—Insulin stimulates glucose uptake in skeletal muscle and adipose tissues primarily by stimulating the translocation of vesicles containing a facilitative glucose transporter, GLUT4, from intracellular compartments to the plasma membrane. The formation of stable soluble *N*-ethyl-maleimide–sensitive fusion protein [NSF] attachment protein receptor (SNARE) complexes between vesicle-associated membrane protein-2 (VAMP-2) and syntaxin-4 initiates GLUT4 vesicle docking and fusion processes. Additional factors such as munc18c and tomosyn were reported to be negative regulators of the SNARE complex assembly involved in GLUT4 vesicle fusion. However, despite numerous investigations, the positive regulators have not been adequately clarified.

RESEARCH DESIGN AND METHODS—We determined the intracellular localization of DOC2b by confocal immunofloresccent microscopy in 3T3-L1 adipocytes. Interaction between DOC2b and syntaxin-4 was assessed by the yeast two-hybrid screening system, immunoprecipitation, and in vitro glutathione S-transferase (GST) pull-down experiments. Cell surface externalization of GLUT4 and glucose uptake were measured in the cells expressing DOC2b constructs or silencing DOC2b.

RESULTS—Herein, we show that DOC2b, a SNARE-related protein containing double C2 domains but lacking a transmembrane region, is translocated to the plasma membrane upon insulin stimulation and directly associates with syntaxin-4 in an intracellular Ca^{2+}-dependent manner. Furthermore, this process is essential for triggering GLUT4 vesicle fusion. Expression of DOC2b in cultured adipocytes enhanced, while expression of the Ca^{2+}-interacting domain mutant DCO2b or knockdown of DOC2b inhibited, insulin-stimulated glucose uptake.

CONCLUSIONS—These findings indicate that DOC2b is a positive SNARE regulator for GLUT4 vesicle fusion and mediates insulin-stimulated glucose transport in adipocytes. ***Diabetes* 58: 377–384, 2009**

From the [1]Division of Endocrinology, Metabolism, Hematological Sciences, and Therapeutics, Department of Bio-Signal Analysis, Yamaguchi University Graduate School of Medicine, Ube, Japan; and the [2]Division of Molecular Metabolism and Diabetes, Tohoku University Graduate School of Medicine, Sendai, Japan.

Corresponding author: Dr. Masahiro Emoto, emotom@yamaguchi-u.ac.jp.

Received 3 March 2008 and accepted 17 November 2008.

Published ahead of print at http://diabetes.diabetesjournals.org on 25 November 2008. DOI: 10.2337/db08-0303.

Additional information for this article can be found in an online appendix at: http://dx.doi.org/10.2337/db08-0303.

Insulin stimulates glucose uptake in skeletal muscles and adipose tissues primarily by stimulating the translocation of vesicles containing a facilitative glucose transporter, GLUT4, from intracellular compartments to the plasma membrane (1,2). In addition to this translocation step, membrane fusion processes are also controlled by insulin (3,4). Like other regulated exocytotic processes in many cell types, the formation of stable soluble *N*-ethyl-maleimide–sensitive fusion protein [NSF] attachment protein receptor (SNARE) complexes between vesicle-associated membrane protein-2 (VAMP-2) and syntaxin-4 initiates GLUT4 vesicle docking and fusion processes (5). However, the precise mechanism by which insulin regulates SNARE complex assembly remains poorly understood.

In neurons, Ca^{2+} triggers exocytotic membrane fusion of synaptic vesicles to the plasma membrane, and calcium sensor proteins such as synaptotagmins have critical roles in this process (6,7). Similar mechanisms result in GLUT4 vesicle fusion in adipocytes and muscle cells. Whitehead et al. (8) demonstrated, and we confirmed, that reduction of intracellular Ca^{2+} ($[Ca^{2+}]_i$) using the membrane-permeable Ca^{2+}-chelating agent BAPTA-AM diminished insulin-stimulated glucose transport, whereas this reagent did not inhibit GLUT4 translocation to the plasma membrane (i.e., GLUT4 vesicle trafficking was not impaired) (8) (N.F., M.E., unpublished observation). These observations suggest that an appropriate intracellular Ca^{2+} level may be required for the final docking/fusion steps of GLUT4 vesicles in adipocytes.

The universal role of Ca^{2+} as a trigger for regulated exocytosis predicts the existence of conserved proteins capable of activating the fusion machinery upon binding Ca^{2+}. Although many proteins have been suggested to play such a role, synaptotagmins have attracted the most attention as putative calcium sensor proteins functioning in regulated exocytosis (9). Synaptotagmin family proteins have tandem C2 domains at the C-terminus. These two domains, C2A and C2B, are conserved in all 13 synaptotagmins described to date and constitute Ca^{2+}-binding modules (10). Many proteins have been identified as being involved in the GLUT4 vesicle fusion machinery in adipocytes. However, neither synaptotagmins nor other calcium sensor proteins have as yet been reported to regulate GLUT4 vesicle fusion.

We investigated, in detail, the mechanisms of Ca^{2+}-dependent GLUT4 vesicle fusion in adipocytes. We searched for double C2 domain proteins as candidate Ca^{2+} sensor proteins suitable for the relatively slow (on the order of several minutes) SNARE complex formation, and we found that DOC2b bound syntaxin-4 upon insulin stimulation in an intracellular Ca^{2+}-dependent manner and

mediated GLUT4 vesicle fusion. DOC2b may be a downstream target of the insulin signal and a positive regulator of SNARE assembly involving regulated exocytosis in adipocytes.

RESEARCH DESIGN AND METHODS

Mouse DOC2a and DOC2b cDNA constructs were kindly provided by Dr. R.R. Duncan (University of Edinburgh, Edinburgh, U.K.). Mouse munc18c cDNA construct was kindly provided by Dr. T. Takuma (School of Dentistry, Health Sciences University of Hokkaido, Hokkaido, Japan).

Cell culture. 3T3-L1 fibroblasts were grown in Dulbecco's modified Eagle's medium (DMEM) with 10% fetal bovine serum (FBS) at 37°C. The cells (3–5 days after confluence) differentiated into adipocytes with incubation in the same DMEM, containing 0.5 mmol/l isobutylmethylxanthine, 0.25 μmol/l dexamethasone, and 4 μg/ml insulin, for 3 days and were then grown in DMEM with 10% FBS for an additional 5–8 days.

Plasmids and antibodies. Wild-type DOC2b was subcloned into peGFP-C2, pDsRed2-C1 (Clontech, Palo Alto, CA), and pGEX-6P1 (GH Healthcare, Buckinghamshire, U.K.) vectors. Calcium interacting domain mutants (CIMs) of DOC2b (D157N, D163N, D297N, and D303N) were subcloned into peGFP-C2 and pGEX-6P1 vectors. We also constructed syntaxin-4 and a series of deletion mutants of DOC2b corresponding to Δmunc13 interaction domain (MID) (amino acids 36–413), ΔC2A (2–120 and 252–413), and ΔC2B (2–264) in a peGFP-C2 vector. Myc-tagged DOC2b (wild-type or CIM) was subcloned into a pcDNA3 vector. All chemically synthesized and PCR-derived DNA sequences were verified by DNA sequencing.

Rabbit polyclonal DOC2b antibody was generated against the peptide sequence CGARDDDEDVDQL specific for DOC2b isoform. This antibody was found to cross-react minimally (online appendix Fig. S1 [available at http://dx.doi.org/10.2337/db08-0303). The following antibodies were used: monoclonal anti-GLUT4 (clone 1F8) (R&D systems, Minneapolis, MN), polyclonal anti-GLUT4, anti-GST (Santa Cruz Biotechnology, Santa Cruz, CA), anti-myc (clone 9E10) (Covance, Princeton, NJ), polyclonal anti–syntaxin-4 (Synaptic Systems, Gottingen, Germany), and fluorescent-conjugated and horseradish peroxidase–conjugated secondary antibodies (Jackson Immuno Research, West Grove, PA).

DOC2b shRNA construct. Short-hairpin RNA (shRNA) specific for mouse DOC2b was designed to have a 5′-GCCAGATGTAGACAAGAAATC-3′ sequence. Synthetic complementary single-stranded DNA of the target sequence was annealed, and the double-stranded DNA was inserted into a pcPUR+U6i cassette (11). This shRNA decreased DOC2b protein expression to 10–20% of the control level within 74 h. A same cassette encoding nonspecific scramble sequence was used as a negative control.

Preparation of recombinant adenovirus vectors. Adenovirus producing enhanced green fluorescent protein (eGFP), myc-tagged DOC2b (wild type, CIM mutant), and shRNA (DOC2b, control) were prepared using an AdEasy adenovirus vector system according to the manufacturer's instructions (Stratagene, Cedar Creek, TX). All amplified viruses were purified by the cesium chloride centrifugation method and stored at −80°C.

Live cell imaging of DOC2b. The peGFP-DOC2b was electroporated into 3T3-L1 adipocytes, which were then reseeded onto 0.1-mm glass-bottom dishes (Matsunami, Tokyo, Japan). At 24–48 h after electroporation, cells were serum starved for 3–4 h in DMEM and then incubated at 37°C for 2 h in Krebs-Ringer HEPES buffer (130 mmol/l NaCl, 5 mmol/l KCl, 1.3 mmol/l $CaCl_2$, 1.3 mmol/l $MgSO_4$, 25 mmol/l HEPES [pH 7.4]). The cells were treated with 100 nmol/l of insulin at 37°C for the time indicated and observed by laser confocal microscopy (LSM510 Pascal; Carl Zeiss, Oberkochen, Germany). For the translocation analysis, fluorescent intensities at three distinct areas in plasma membrane, cytosol, and nucleus (nine areas per cell each) of three independent cells were analyzed by Photoshop software CS2.

Yeast two-hybrid screening. The Matchmaker Yeast Two-Hybrid System (Clontech) was used for determination of DOC2b-binding partners. Full-length DOC2b and munc18c cDNA were subcloned into a pLexA vector and full-length syntaxin-4 and munc18c cDNA into a pB42AD vector. A standard lithium acetate/single-stranded carrier DNA/polyethylene glycol method for transformation into yeast strain EGY48 (p8op-lacZ) was used, and these proteins were expressed in this strain. Transcriptional activation of LacZ was determined by an X-Gal assay. β-Galactosidase activity was detected within 16 h of reaction at 30°C.

In vitro GST pull-down assay. Glutathione S-transferase (GST) fusion proteins of wild-type and CIM DOC2b were purified according to the manufacturer's instructions. GST syntaxin-4 was cleaved with PreScission Protease (2 units/μl) (GH Healthcare) in buffer containing 50 mmol/l Tris-HCl (pH 7.0), 150 mmol/l NaCl, 1 mmol/l EDTA, and 1 mmol/l dithiothreitol at 4°C for 16 h. At the end of incubation, cleaved syntaxin-4 protein was further purified using Amicon Ultra filter devices (Millipore, Danvers, MA).

Recombinant individual GST-DOC2bs or GST (1 μg each) were incubated with 1 μg of recombinant syntaxin-4 in 1 ml of Tris-buffered saline (20 mmol/l Tris, pH 7.4, 150 mmol/l NaCl) plus 0.5% Triton X-100 in the presence of 2 mmol/l EDTA or 1 mmol/l $CaCl_2$ for 4–6 h. This mixture was immunoprecipitated by incubating with Glutathion Sepharose 4B (GE Healthcare) for 1 h. The precipitates were washed four times and analyzed by SDS-PAGE and immunoblotting. Approximately 5% of syntaxin-4 was pulled down by the GST-DOC2b.

Northern blotting. Total RNAs were prepared from 3T3-L1 fibroblasts, 3T3-L1 adipocytes (days 3 and 9 of differentiation) or rat epididymal fat, and mouse brain using ISOGEN (Nippongene, Tokyo, Japan) and denatured in formaldehyde/formamide, resolved by electrophoresis, and transferred to hybond-N membranes (GH Healthcare). The membranes were hybridized with α-[^{32}P]–labeled full-length DOC2a and DOC2b cDNAs as probes and then washed three times with 1× saline sodium citrate buffer (15 mmol/l NaCl, 15 mmol/l sodium citrate [pH 7.0], and 0.1% SDS) at 65°C. Radioisotopic measurements were conducted using a Phosphorimager FLA2000 (Fuji film, Tokyo, Japan).

Immunoprecipitation and immunoblotting. A 10-cm plate of cells was lysed in 1 ml of lysis buffer (20 mmol/l HEPES [pH 7.2], 100 mmol/l NaCl, 25 mmol/l NaF, 1 mmol/l sodium vanadate, 1 mmol/l benzamidine, 5 μg/ml leupeptin, 5 μg/ml aprotinin, 1 mmol/l phenylmethylsulphonyl fluoride, 1 mmol/l dithiothreitol, and 0.5% NP-40) in the presence of 2 mmol/l EDTA or 1 mmol/l $CaCl_2$ and centrifuged for 15 min at 15,000*g*. The postnuclear lysates were used for the following experiments. The protein concentration was measured with a bicinchoninic acid protein assay reagent (Pierce, IL). For immunoprecipitation, the cell lysates were preincubated with protein-G/A–Sepharose at 4°C for 30 min to remove nonspecific bound proteins. Then, samples were incubated with primary antibodies at 4°C for 8–12 h followed by incubation with protein-G/A–Sepharose. Lysates and immunoprecipitates were resolved by SDS-PAGE and transferred to a polyvinylidene fluoride membrane (GH Healthcare). The membranes were incubated with primary antibodies for 8–12 h. Protein signals were visualized using horseradish peroxidase–conjugated secondary antibodies and an enhanced chemiluminescence substrate kit (GH Healthcare). The efficiencies of immunoprecipitation of the associated protein in Fig. 3*C–E* were ~1, 0.5, and 0.6%, respectively. All the images in figures are representative, and we repeated the immunoblots at least three times and found similar results.

Immunofluorescence microscopy and digital image analysis. Differentiated 3T3-L1 adipocytes were left untreated or electroporated by eGFP-DOC2b (wild type, CIM, ΔMID, ΔC2A, and ΔC2B), eGFP alone, DsRed2-DOC2b (wild type, CIM), shRNAs (control, DOC2b), or myc-GLUT4-eGFP. The cells were then replated onto coverslips and allowed to recover for 48 h. Cells were preincubated in the presence or absence of 50 μmol/l of BAPTA-AM for 10 min, followed by incubation with or without insulin for 20 min at 37°C. Next, the cells were fixed with 3.7% formaldehyde in PBS and permeabilized with buffer A (0.5% Triton X-100, 1% FBS in PBS) for 15 min. For the detection of endogenous proteins, the coverslips were incubated for 2 h with primary antibodies at room temperature. The cells were washed and incubated with an appropriate secondary antibody for 30 min. The coverslips were washed thoroughly again and mounted on glass slides. Immunostained cells were observed at room temperature with an LSM 5 PASCAL laser-scanning confocal microscope and its two-channel–scanning module (Carl Zeiss) equipped with an inverted Zeiss Axiovert 200M using the 63× oil objective lens (numerical aperture 1.4) run by LSM 5 processing software and Adobe Photoshop CS2. At least five cells were observed in a condition. The experiments were repeated at least three times, unless stated otherwise. All the images in figures are representative, and the conclusions are based on qualitative visual impression. The cell surface myc-GLUT4-eGFP was measured by subtracting the internal myc signal from total myc signal of electroporated cells. The plasma membrane eGFP content was also measured. The cell surface GLUT4 was calculated as (total myc − internal myc)/(total eGFP − internal eGFP) (22).

2-Deoxy-glucose uptake. Differentiated adipocytes were prepared in 24-well plates. Cells were infected with the recombinant adenoviruses. Two days thereafter, the cells were serum starved for 2 h at 37°C in Krebs-Ringer HEPES buffer. Then, the cells were stimulated with or without 100 nmol/l of insulin for 10 min, and 2-deoxy-glucose uptake was determined by 2-deoxy-D-[2,6 ^{3}H] glucose incorporation. Nonspecific glucose uptake was measured in the presence of 20 μmol/l cytochalasin B and subtracted from each determination to obtain specific uptake. The results were normalized by the protein amount.

Statistical analysis. Multiple comparisons among groups were performed using one-way ANOVA (post hoc test: Tukey-Kramer). Results are presented as means ± SD. Values of $P < 0.05$ were considered statistically significant.